Biological mechanisms underlying priming of vascular plant material in the presence of diatoms

Patricia Bonin, Aurélie Portas, Julie Hardy, Sophie Guasco, Ts Bianchi, Nd Ward, Jf Rontani

Aquatic Microbial Ecology

Manuscript:	AME-0-00-000
Title:	Biological mechanisms underlying priming of vascular plant material in the presence of diatoms
Authors(s):	Patricia Bonin (Corresponding Author), Aurelie Portas (Co-author), Julie Hardy (Co-author), Sophie Guasco (Co-author), Thomas S Bianchi (Co-author), Nicholas Ward (Co-author), Jean-Francois Rontani (Co-author)
Keywords:	13C-labelling, Algal-bacterial interaction, Bacterial biodegradation, Bacterial diversity, Coastal marine diatom, DNA-SIP analyses, Particle-associated bacteria, Particulate organic carbon, Priming Effect
Type:	Research Article

Biological mechanisms underlying priming of vascular plant material in the presence of diatoms

Patricia Bonin[1]*, Aurélie Portas[1], Julie Hardy[1], Sophie Guasco[1], Thomas S. Bianchi[2], Nicolas D. Ward[3,4], Jean-FrançoisRontani[1]

[1]Aix Marseille Univ, Université de Toulon, CNRS, IRD, MIO UM 110, Marseille, France, 13288, Marseille, France

[2]Department of Geological Sciences, Box 112120, University of Florida, Gainesville FL 32611-2120, USA

[3]Marine and Coastal Research Laboratory, Pacific Northwest National Laboratory, 1529 W Sequim Bay Rd, Sequim, WA, USA, 98382

[4]School of Oceanography, University of Washington, Box 355351, Seattle, WA, USA, 98195

Running head: Experimental priming of TPOM by marine diatoms

Keywords: Priming Effect; bacteria; DNA-SIP analyses; ^{13}C-labelling; *Avena sativa*; *Skeletonema costatum*; Rhône SPM; lipids.

* Corresponding author. E-mail address: patricia.bonin@mio.osupytheas.fr (J.-F. Rontani).

Abstract

Our understanding on the fate of terrigenous material in the coastal ocean is, in part, limited by a lack of mechanistic information on how diverse microbial consortia interact with organic substrates with varying degrees of reactivity. Here, we report results from a laboratory incubation experiment in seawater collected from the Gulf of Marseille, amended with ^{13}C-labelled terrestrially-derived particulate organic matter (TPOM), Rhône River suspended particulate matter (SPM) as inoculum, and the diatom *Skeletonema costatum* as a reactive substrate. We monitored ^{13}C-labelled TPOM lipid tracers (long-chain fatty acids, *n*-alkan-1-ols, phytol, sitosterol, β-amyrin and components of cutins) throughout a 42-day incubation experiment. Incubation treatments were amended with diatom biomass within the range of diatom concentrations found in estuaries bordering the Gulf to test for priming effects on TPOM degradation. Both DNA stable isotope probing (DNA-SIP) and ^{13}C of microbial fatty acids were used to link microbes with decomposition of labelled TPOM. Comparisons with controls, carried out without diatom additions, showed faster decay of phytol, *n*-alkan-1-ols, and components of cuticular waxes in the presence of diatoms, while fatty acids and sitosterol were unaffected. Bacteria belonging to the Bacteroidota phylum (mainly *Flavobacteria* and *Cytophaga*) were the dominant microbes involved in priming-induced TPOM degradation in the incubation treatments. Sphingomonadales and Rhizobiales, capable of lignin and hemicellulose degradation, also contributed to the degradation of TPOM, but did not seem to contribute to priming effects related to increased diatom abundance. These lab-based results demonstrate that priming of TPOM occurred selectively via a consortium of microbes, rather than enhanced production of extracellular enzymes by one bacterial taxon.

Introduction

Rivers export substantial amounts of terrestrially-derived particulate organic matter (TPOM) to the coastal ocean (e.g., Berner 1982, Hedges et al. 1997). However, there remain critical gaps in our understanding of the complex and dynamic mechanisms controlling the fate of this material along the river-ocean continuum (e.g., Ward et al. 2017). Organic molecules associated with higher plants such as lignocellulose have historically been considered recalcitrant to marine microbial decay pathways (de Leeuw & Largeau 1993; Hedges 2002; Bianchi et al. 2013). Interestingly, early work also showed that coastal marine sediments stored less TPOM than predicted from global river inputs (Hedges & Keil 1995). This implied that TPOM global budgets were either incorrect, or that TPOM experienced greater degradation than expected in coastal waters, and/or was exported to offshore waters more than expected (Hedges et al. 1997; Burdige 2005; Bianchi 2011). More recently, this paradigm has changed showing that TPOM can, in fact, be substantially decomposed by microbes in coastal waters (e.g., Vonk et al. 2010; Bourgeois et al. 2011; Karlson et al. 2011; Rontani et al. 2014; Bianchi et al. 2018). However, the diversity of microorganisms and metabolic pathways responsible for TPOM decay (Pointing & Hyde 2000; Bjordal 2012) and their relative role in pre- and post-depositional processes that control TPOM stocks in the coastal ocean remain largely unexplained.

Coastal TPOM degradation is likely carried out by a consortium of microbial communities with different metabolic functions and enzymes. The dynamic nature of the coastal zone can result in complex relationships whereby TPOM-degrading microbial distribution patterns are not actually linked with TPOM concentration gradients. For example, Gammaproteobacteria, which are abundant in TPOM-depleted saline waters, were found to be more efficient at degrading TPOM than Betaproteobacteria, which dominate TPOM-rich river waters (Newton et al. 2011; Bonin et al. 2019). The decay of TPOM may also be enhanced by unique interactions between different metabolic pathways across steep physicochemical

gradients, or aquatic critical zones (Bianchi & Morrison 2018), where turbid nutrient-rich river waters interface with phytoplankton-rich marine waters. Finally, although marine fungi (e.g., Ascomycetes) have long been recognized for their capability of decomposing TPOM in coastal waters (Jones & Irvine 1971; Benner et al. 1984; Mouzouras 1989), they have largely been ignored in coastal carbon cycling, but with some recent renewed interests (Pointing & Hyde, 2000; Blanchette 2010; Byordal & Dayton, 2020).

The term "priming effect" more broadly describes a suite of interactive microbial processes (e.g., Bengtsson et al. 2018). While well-studied and demonstrated in soils (Parnas 1976; Kuzyakov et al. 2000; Bastida et al. 2019), priming effects are less constrained in aquatic systems, and are generally described as an enhanced remineralization of terrestrially-derived material in the presence of labile co-substrates from algal sources (e.g., Guenet et al. 2010, 2014; Bianchi et al. 2011, 2015; Steen et al. 2016; Ward et al. 2019; Aller & Cochran 2019). Inconsistencies in the detection of priming in aquatic systems may, in part, be related to the diversity of indices used to "track" priming (e.g., change in CO_2, nutrient production/uptake, bacterial production, enzyme assays, loss of primed substrate) and/or where the work was conducted (e.g., field or laboratory) (Sanches et al. 2021). Nevertheless, priming of recalcitrant OM in aquatic systems is generally hypothesized to result from: (i) an increase of microbial biomass due to consumption of reactive substrates (algal components) (Grant & Betts 2004), or (ii) an enhanced microbial production of extracellular enzymes capable of breaking less reactive substrates (TPOM components), driven by energy obtained from the breakdown of more reactive substrates (e.g., amino acids and simple sugars) (e.g., Guenet et al. 2010, Ward et al. 2016). Coastal deltaic regions, characterized by a high input of TPOM, high rates of primary production, and high respiration rates via microbial communities, are generally considered to have a high priming potential (Guenet et al. 2010; Bianchi 2011). Unfortunately, the specific mechanistic pathways involved in the degradation of primed TPOM in aquatic systems remains

poorly understood (Bengtsson et al. 2018; Sanches et al. 2021). Such knowledge may be critical for accurately portraying how coastal biogeochemical dynamics (e.g., carbon fluxes and nutrient cycling) influence global climate in next generation Earth System Models (Ward et al. 2020; Bianchi et al. 2021).

A recent experiment observed enhanced TPOM degradation of suspended particulate matter (SPM) in the Rhône River after a phytoplankton bloom dominated by diatoms based on specific lipid tracer analyses (amyrins, lupeol, phenolic acids, and components of cuticular waxes) (Bonin et al. 2019). This enhanced TPOM biodegradation might be attributed to the presence of diatoms, however, due to the use of distinct SPM inocula during these experiments this enhancement may have also resulted from the presence of a more efficient bacterial community during the bloom period (Bonin et al. 2019). Thus, the role of priming effects on TPOM degradation in this ecosystem could not be unequivocally demonstrated. Building on this previous work, ^{13}C-labelled *Avena sativa* ("common" oat, a C_3 grass - widespread throughout the Rhône River; Lecornu & Michel, 1986), was incubated in the dark in natural seawater, in the presence and absence of the marine diatom *Skeletonema costatum,* supplemented with SPM collected in the Rhône River. The seawater and SPM served as marine and terrestrial bacterial inoculum, respectively. Quantification of labelled lipid tracers allowed us to better track the priming of river-borne TPOM remineralization in the presence of marine diatom material. Measurement of ^{13}C-incorporation in bacterial and fungal fatty acids, along with DNA-SIP analyses, allowed for the identification of the dominant microbes involved in the enhanced degradation of TPOM to test the hypothesis that priming-induced TPOM degradation involves a diversity of microbial actors.

Materials and methods

Sampling

Fresh SPM samples were collected using a Teflon-coated high-speed centrifuge (CEPA Z61) at the Arles station of the MOOSE program (43°40'44"N, 4° 37'16"E) (at 30 km upstream the Rhône River mouth) on 17 December 2018. SPM samples were transported in an ice box to the laboratory and then stored at 4°C until further analysis. Seawater samples, for lab incubations, were collected on 7 December 2018 at the station SOLEMIO (SOMLIT network) (43° 14' 30"N, 5° 17' 30"E) (in the Gulf of Marseille) and filtered through GF/F (0.8 µm) before its use. At the time of sampling, the salinity was 38 g kg^{-1} (measured using an ATAGO ATC refractometer).

Substrate

^{13}C labelled (97% ^{13}C) leaves of *A. sativa* were obtained from IsoLife (Wageningen, The Netherlands). Leaves were cut into small pieces and then ground in a Fast Prep-24^{TM} 5G (MP Biomedicals), using metal beads (2 mm diameter).

Biodegradation experiments

Incubation experiments were performed in a growth chamber at a controlled temperature of 15°C – temperature of ambient coastal waters at the time of sampling. Experimental systems were composed of 10 mg of ^{13}C labelled *Avena sativa*, 650 µL of a culture of *Skeletonema costatum* containing 1.1 x 10^6 cells mL^{-1}, 150 mg of fresh SPM collected at the Arles station and 150 mL of seawater. The diatom concentrations used here (4.8 x 10^3 cells mL^{-1}) corresponded to the range of nanophytoplankton in the Rhône Estuary (from 2 x 10^3 to 3 x 10^4 cells mL^{-1}) (Obernosterer et al. 2005). To maintain aerobic conditions, Erlenmeyer flasks, coated with cotton plugs, were incubated in the dark on a reciprocal shaker (96 rpm, 5 cm amplitude). At each sampling times (0, 7, 15, 28 and 42 days), 3 flasks (triplicates) were

sampled for lipid analyses and 3 for SIP analyses. Control flasks without diatoms were also carried out in triplicate and incubated for 14 and 42 days. All samples were filtered on pre-combusted GF/F filters (Whatman) for chemical analyses and on 0.2 µm Nuclepore filters (Whatman) for SIP analyses and stored at −20°C until further analysis. Chemical analyses were only carried out on the controls incubated for 42 days.

Chemical analyses

Lipid extraction

For lipids, thawed filters were placed in methanol (20 mL) with excess $NaBH_4$ (70 mg; 30 min at 20°C). This process was conducted to reduce any hydroperoxides in samples (Galeron et al. 2015), which are known to induce autoxidative damage of some lipids during the hot saponification step. After $NaBH_4$ reduction, 20 mL of water and 2.8 g KOH were added and directly saponified by refluxing (75°C) for 2 h. After cooling, samples were acidified with HCl (pH 1) and extracted (3×) with dichloromethane (DCM). The combined DCM extracts were dried over anhydrous Na_2SO_4, filtered, and concentrated by rotary evaporation at 40 °C to isolate the total lipid extract (TLE).

Derivatization

TLEs were taken up in 300 µL of a mixture of pyridine and N,O-bis(trimethysilyl)trifluoroacetamide (BSTFA; Supelco) (2:1, v:v) and silylated for 1 h at 50°C to convert OH-containing compounds to their TMSi-ether derivatives. After evaporation to dryness under a stream of N_2, derivatized residues were taken up in a mixture of ethyl acetate and BSTFA (to avoid desilylation of fatty acids) for analysis using gas chromatography-EI quadrupole time of flight mass spectrometry (GC-QTOF).

Gas chromatography–EI quadrupole time of flight mass spectrometry

Accurate mass measurements were carried out in full scan mode using an Agilent 7890B/7200 GC/QTOF System (Agilent Technologies, Parc Technopolis – ZA Courtaboeuf, Les Ulis, France) and a cross-linked 5% phenyl-methylpolysiloxane (Macherey-Nagel; OPTIMA-5MS Accent) (30 m x 0.25 mm, 0.25 µm film thickness) capillary column. Analyses were performed in pulsed splitless mode set at 270 °C, where oven temperature was ramped from 70 °C to 130 °C at 20 °C min^{-1} and then to 300 °C at 5 °C min^{-1}. The pressure of the carrier gas (He) was maintained at 0.69 x 10^5 Pa until the end of the temperature program. Instrument temperatures were 300 °C for the transfer line and 230 °C for the ion source; nitrogen (1.5 mL min^{-1}) was used as collision gas. Accurate mass spectra were recorded across the range *m/z* 50–700 at 4 GHz with the collision gas opened. The QTOF-MS instrument provided a typical resolution ranging from 8009 to 12252 from *m/z* 68.9955 to 501.9706. Perfluorotributylamine (PFTBA) was used for daily MS calibration. Compounds were identified by comparing their TOF mass spectra, accurate masses and retention times with those of ^{12}C standards. Quantification of each compound involved extraction of specific accurate fragment ions, peak integration and determination of individual response factors using external standards and Mass Hunter software (Agilent Technologies, Parc Technopolis – ZA Courtaboeuf, Les Ulis, France).

High resolution accurate mass full scans, obtained from GC-QTOF analyses, allowed for estimation of isotopic enrichment states of all lipids measured (Triebl & Wenk 2018).

Standards

^{13}C-labelled lipids were quantified using GC-QTOF with external ^{12}C-standards. Sitosterol, nonadecanoic acid, hexacosan-1-ol and phytol, were obtained from Sigma-Aldrich. Fatty acids and *n*-alkan-1-ols, were quantified with standards of nonadecanoic acid and hexacosan-1-ol, respectively. It is well-known that epoxides undergo alcoholysis to

methoxyhydrins, hydrolysis to diols during alkaline hydrolysis, and are converted to chlorohydrins during acidification with HCl (Marchand & Rontani 2001). The degradation products of 9,10-epoxy-18-hydroxyoctadecanoic acid thus formed and 9,16- and 10,16-dihydroxyhexadecanoic acids were quantified with a standard mixture of 9- and 10-hydroxyoctadecanoic acids produced from oleic acid in three steps: (i) photosensitized oxidation of oleic acid in pyridine in the presence of hematoporphyrin as sensitizer, (ii) $NaBH_4$-reduction of the resulting allylic hydroperoxyacids, and (iii) hydrogenation of the double bond in methanol with Pd/C as catalyst.

DNA and Sequencing

DNA-SIP analyses

DNA stable isotope probing and metabarcoding sequencing were used to assess what bacteria were involved in ^{13}C- *A. sativa* degradation in the presence of ^{12}C- *S. costatum* as a co-substrate. After the growth of microorganisms in the presence of the substrate (^{13}C- *A. sativa*) and co-substrate (^{12}C- *S. costatum),* ^{13}C-DNA was separated from ^{12}C-DNA by isopycnic density gradient centrifugation in CsCl gradients. Within the gradient from lightest to heaviest DNA, microorganisms that consume only ^{12}C -*S. costatum,* then both ^{12}C- *S. costatum* and ^{13}C- *A. sativa* and finally only ^{13}C- *A. sativa* were explored. Five fractions of increasing density were separated from each sample and submitted to Mi-seq sequencing. SIP analyses were carried out on the samples collected after 0, 7, 14, 28 and 42 days of incubation in the presence of ^{12}C- *S. costatum* and after 14 and 42 days of incubation without ^{12}C- *S. costatum*.

DNA extraction and isopycnic separation

For each stop time, samples (individual vials) were filtered on 0.22 μm sterile filters and stored frozen at -80°C until further analysis. Each filter was treated with TE-Lysis buffer (20 mM Tris, 25 mM EDTA, 1 μg mL^{-1} Lysozyme) followed by 1% SDS treatment. Extractions were performed twice with an equal volume of phenol-chloroform-isoamyl alcohol (25:24:1, v:v:v) pH 8, followed by a treatment with chloroform-isoamyl alcohol (24:1, v/v), DNA precipitation by isopropanol and resuspension in 50 μL of molecular biology grade water. Extracted DNA was quantified using the Qubit double-stranded DNA (dsDNA) high-sensitivity assay kit and a Qubit 2.0 fluorometer (Invitrogen, Eugene, OR, USA).

The ^{13}C-DNA was separated from community ^{12}C-DNA by CsCl gradient centrifugation in the presence of EtBr (Lueders et al. 2003; Neufeld et al. 2007). To separate DNA by density, 10 μg of DNA was added to approximately 5.4 mL of a saturated CsCl and gradient buffer (100 mM Tris-HCl, 100 mM, KCl 0.1 M, EDTA 1 mM) and 110 μL of a stock solution 10 mg mL^{-1} EtBr in a 5.5 mL OptiSeal ultracentrifuge tube (Beckman Coulter, Fullerton, CA, USA). The final density of the solution was 1.725 g mL^{-1}. The samples were spun in an Optima XPN ultracentrifuge (Beckman Coulter, Fullerton, CA, USA) using a Beckman ntv-90 rotor at 127,000 g for 40 h at 20°C. After centrifugation, gradients of density-separated DNAs were fractionated, and ten fractions (ca. 500 μL) were collected per tube and weighed on a digital balance (precision 10^{-4} g) to confirm gradient formation. EtBr was removed by three successive washings with TE (10 mM Tris-HCl, 1 mM EDTA, pH 8)-butanol (50:50, v/v). The distribution of DNA in CsCl gradients was quantified by spectrophotometry (BioSpec-nano, Shimadzu). Five fractions of DNA were obtained from the heaviest (E) to the lightest (A) with BDs of ~ 1.755–1.740, 1.740–1.730, 1.730–1.720, 1.720–1.710 and 1.710–1.700 g mL^{-1}. DNA was precipitated with 800 μL polyethylene glycol 6000 (1.6 M) overnight at room temperature, recovered by centrifugation 45 min at 13,000 g, washed once with 500 μL 70% (v/v) ethanol, suspended in 20 μL sterile deionized water and then stored at -20°C.

Twenty-five samples of DNA ^{13}C-SIP experiment incubated with and without amendment of ^{12}C- *S. costatum* were sequenced. The V4 region of the bacterial and archaeal 16S rRNA genes were amplified using universal primer sets (Caporaso et al. 2012), 515F-Y (5′-GTGYCAGCMGCCGCGGTAA-3′, Parada et al. 2016) and 806RB (5′-GGACTACNVGGGTWTCTAAT-3′, Apprill et al. 2015) (0.5 µM) and 2.5 U TaKaRa PrimeSTAR® GXL DNA polymerase (OZYME) in reactional system of 50 µL as described in Garel et al. (2019). The 16S amplicons were sequenced by the MiSeq Illumina (paired end 2* 250) platform Get of Genotoul (INRA, Narbonne France, https://get.genotoul.fr).

Sequence data processing

The program *dada2* (version 1.18) (Callahan et al. 2016) using default settings to correct sequence errors, in the R software version 3.4.3) was used to identify unique amplicon sequence variants (ASVs) from raw sequence reads. Using the function *filterAndTrim*, forward and reverse primer sequences were removed, maxEE was set to 2, trunQ was set to 11, maxN was set to 0. The function *orient.fwd* was used to orient sequences in the same direction. Error rates of forward and reverse reads were modeled with *learnerrors* for 100 Million bases. Paired ends were merged with *mergePairs* and unique sequences were inferred with the function *dada*. Chimeras were removed with *removeBimeraDenovo* using the "consensus" method. Taxonomy was assigned to the output sequences through the Silva database (version 138, Quast et al. 2012). The *phyloseq* package (McMurdie et al. 2013) was used to combine, analyze, and graphically display ASV tables. Raw sequence data were deposited to BioProject PRJ XXXX.

To select the more differentially abundant genera, data were first converted in percentage with the *transform_sample_count* function from phyloseq package version 1.16.2 and then aggregated by genus with *aggregate_taxa* from the same package. To detect difference, another filter was used with *Aggregate_rare* function follows by the parameters of detection equal to

1/100 and prevalence equal to 66/100. To visualize associations between different sources of data sets and reveal potential patterns ComplexHeatmap package was applied. Vizualisation was based on the z-score of each genus (i.e. the distance from the mean abundance, expressed in number of standard deviations, by row). A boxplot representing the relative abundance of each genus (expressed as log) was generated and included on the heatmap plot, by the *row_anno_boxplot* and *rowAnnotation* functions.

Co-occurrence networks were built from the communities incubated in the presence of ^{12}C- *S. costatum*. The network analysis used in inputs data converted in percentage with "transform_sample_counts" function and aggregated by Genus with "*aggregate_taxa*". Only specific phyla were selected: Proteobacteria, Bacteroidota, Planctomycetota, Cyanobacteria and Verrumicrobiota. Three networks were computed, one for each density band (A; B-C and D-E). The data were correlated with "*trans_network"* function from microeco version 0.4.0 (Liu et al. 2021).

The calculation of the correlation was carried out with WGCNA (Langfelder et Horvath 2008) with a threshold equal to 0.0001 and Spearman for the method of the correlation. Only correlations with a coefficient (rho) > |0.7| were considered for further analysis. To visualize the network, Gephi software version 0.9 was used (Bastian et al. 2009). Nodes represented genera and edges represented the significant correlations between them. The network was defined by weighted correlation network analysis that determined modules (cluster of highly co-occurring microorganisms) and network nodes with regard to module membership.

Specific biodegradation response of the modules was assessed by Spearman's correlations between module eigengenes and the rate of biodegradation of selected compounds eicosanoic acid, docosanoic acid, 9,10-epoxy-18-hydroxyoctadecanoic acid (constituent of vegetable cuticular waxes), phytol, sitosterol, isomeric dihydroxyhexadecanoic acids (constituents of vegetable cuticular waxes), tetracosan-1-ol; hexacosan-1-ol, octacosan-1-ol,

and triacontan-1-ol. To correlate the module and biodegradation rates, the package microeco was used again with the functions "*cal_cor*" to calculate and "*plot_cor*" to visualize.

Results

Lipid composition of *A. sativa* leaves

The main ^{13}C labelled lipid components detected after alkaline hydrolysis of *A. sativa* leaves were hexadecanoic (palmitic), 3-(4-hydroxy-3-methoxyphenyl)prop-2-enoic (ferulic), and (2*E*)-3-(4-hydroxyphenyl)prop-2-enoic (*p*-coumaric) acids (Fig. 1). Smaller amounts of labelled long-chain fatty acids ($C_{20:0}$ and $C_{22:0}$), long-chain *n*-alkan-1-ols (C_{24}-C_{30}), phytol (chlorophyll phytyl side-chain), sitosterol, isomeric 9,16- and 10,16-dihydroxyhexadecanoic acids, degradation products of 9,10-epoxy-18-hydroxyoctadecanoic acid and traces of β-amyrin could be also detected (Supplementary Fig. S1).

Incubation experiments

^{13}C-labelled lipids were quantified after 0, 7, 15, 28 and 42 days of incubation (Table 1, Fig. 1). A degradation of fatty acids, *n*-alkan-1-ols, phytol, sitosterol, and components of cuticular waxes was observed. Interestingly, this degradation occurred without the accumulation of any detectable intermediate catabolites, likely due to their rapid remineralization (e.g., Boetius et al. 1996). The degradation of phytol, C_{24}, C_{26} and C_{28} *n*-alkan-1-ols in controls (without diatoms) incubated for 42 days, appears to be significantly slower than in treatments with diatoms (t-test, $p = 0.01$, $p = 0.01$, $p = 0.002$, $p = 0.03 < 0.05$, respectively). However, the decay of C_{20} and C_{22} fatty acids, cuticular waxes and sitosterol was not significantly different in the presence or absence of diatoms (t-test, $p = 0.19$, $p = 0.21$, $p =$

0.19, p = 0.75 > 0.05, respectively) (Table 1, Fig. 1); there was also no detectable degradation of β-amyrin in any of the incubations.

Bacteria and degradation of *A. sativa*

From 25 density fractions 1,207,563 raw reads were generated, ranging between 88,709 and 20,773 sequences per library (Supplementary Table S1). After the quality trimming process, about 515,689 reads were retained (86%). The Good's index showed that the sequencing depths were sufficient to cover 97.8 ± 3.3% of the microbial diversity and the rarefaction curves approached saturation, indicating an acceptable sequencing depth for all remaining samples. All good quality sequences were distributed into 5164 ASVs. The global species richness (observed ASV counts) ranged from 54 to 106 ASVs depending on the sample.

Phylum and class-level phylogenetic analysis of communities incubated with ^{12}C- *S. costatum* (Fig. 2A) indicated that sequences affiliated with Bacteroidota were highly abundant in the second heaviest fractions (B and C, B-C: 1.710-1.730 g mL^{-1}) (47.01 ± 8.5%), with relative abundances of 3.1−3.4 times higher than the lightest fraction (A) or the mean at T_0. In the heaviest fraction (D and E, D-E: 1.7230-1.755 g mL^{-1}), Bacteroidota abundance was close to that observed in the lightest fraction (21.2 ± 4.9 and 15.3 ± 3.8 %, respectively). The relative abundance of Flavobacteriales reached its highest value after 14 (B) or 28 (C) days of incubation (32.4 ± 5.3%), whereas Cytophagales overabundances were observed after only 7 days (18.9 ± 5.6%). Flavobacteriales and Cytophagales abundances (10.63 ± 3.3% and 3.1 ± 2.7%, respectively) were clearly weaker in the D-E fractions (Fig. 2D).

In most fractions, the relative abundance of Proteobacteria varied only slightly over the time (78.8 ± 6.1, 44.1 ± 9.3 and 57.8 ± 7.5% for the A, B-C and D-E fractions, respectively). Proteobacteria Gammaproteobacteria were dominant in the lightest fraction and thus used mainly the unlabeled algal substrate as a carbon source, whereas Alphaproteobacteria, mainly

found in the heaviest fraction, had clearly consumed the labelled *A. sativa* (Figs. 2B, 2C). In this heaviest fraction, the relative abundance of Planctomycetota and Verrumicrobiota reached 12.8 ± 2.7% (8 fold higher than in A fraction) and 6.5 ± 1.7%, respectively, after 28 days of incubation. Gammaproteobacteria, bacteria affiliated to Nitrosococcales, formerly affiliated to Betaproteobacteria (Fig. 2B), were most abundant in the lightest fraction (A) and increased after 14 days to reach their maximal level (55.5 ± 4.6 % of the total community). The same pattern was observed for the less abundant Salinisphaerales. For the other bacteria belonging to Alteromonadales, Burkholderiales, Cellvibrionales, and Oceanospirillales orders, no significant differences in their distribution within fractions or over the time was observed. In contrast, the relative abundance of Alphaproteobacteria (Fig. 2C) declined with time in the lightest fraction, but was maintained in fractions D-E. Rhizobiales and Sphingomonadales orders were significantly higher abundant in the heaviest fraction (D-E) with 24.4- (D-42d), 47.2- (E-42d) fold higher abundance than those of the unlabeled fraction for the former and 36.5- (D-14-28d), 61.6- (E-28d) for the latter.

To better understand the bacteria involved in the assimilation of the labeled substrates, ^{13}C-incorporation (%) in the main fatty acids (Fig. 3) and hydroxyacids (Fig. 4) was measured during the experiment including chemotaxonomic approaches (Table 2). The labelling was highest in the case of dodecanoic, 12-methyltridecanoic (iso-C_{14}), 13-methyltetradecanoic (iso-C_{15}), hexadec-11-enoic, 2-hydroxy-13-methyltetradecanoic, 3-hydroxy-13-methyl-tetradecanoic, and 3-hydroxy-15-methylhexadecanoic acids.

To disentangle the effect of *S. costatum* as algal co-substrate on individual members of the community, we focused on the two main phyla (Proteobacteria and Bacteroidota) and identify the significantly differentially abundant genera between incubations with and without the diatom, *S. costatum* for the same sampling time 14-days and 42 -days for the A, B-C and D-E fractions, respectively (Fig. 5 and Fig. S2). The z-score pattern of the most discriminant

genera has been used to highlight the preponderant effect of *S. costatum* as co-substrate on bacterial diversity.

Looking across the whole community, the presence of diatoms only affected the relative abundance of a few genera. Except *Methylophaga*, whose relative abundance reached up to 45% of the total community in band A, the genera differentially abundant between incubations with and without diatoms were minor and their relative abundance rarely exceeded 1%. After 14 days of incubation, in the BC band the *Taeseokella, Algoriphagus* and *Flavobacterium* genera belonging to the Bacteroidota were significantly more abundant in the presence of diatoms, while in the DE band *Alteromonas* and *Pseudoalteromonas* were dominant (Fig. 5). After 42 days, only *Erythrobacter* was more abundant in the diatom incubations.

Recent studies show that microbial co-occurrence patterns can help to unveil ecologically meaningful interactions between species (Fillol et al. 2015; Horner-Devine et al. 2007; Steele et al. 2011). To better explore potential microbial consortia involved in the priming of TPOM in the presence of diatoms, we constructed a co-occurrence network based on strong and significant Spearman correlations. Network approaches showed that co-occurring species were often organized into groups, or modules, of functional significance (Barberan et al. 2012; Chaffron et al. 2010; VickMajors et al. 2014). Modules are groups of highly connected genera within the group but with very few connections outside the group. Correlations between modules and the rates of biodegradation of ^{13}C- specific compounds were calculated (Fig. 6 1-5).

As expected, in the lightest band (A) there was no correlation between any module and the degradation of ^{13}C-TPOM markers (Fig. 6-1). The intermediate fractions B-C, contained DNA of bacteria that assimilated both ^{13}C-labelled *A. sativa* and ^{12}C- *S. costatum* and thus played a potential role in the observed priming effects. Modules M4, M5 and M12 represented 9.43, 8.49 and 2.83% of the nodes of the network, respectively (Fig. 6-2, Fig. S3-1), and was

significantly correlated with the degradation of most of the TPOM markers with the exception of waxes (9,10-epoxy-18-hydroxyoctadecanoic acid and Isomeric dihydroxyhexadecanoic acids) (Fig. 6-5). Module M4 grouped 2 genus belonging to cyanobacteria (*Prochlorococcus* and *Synechococcus*) and genus mainly affiliated to Alteromonadales (*Alteromonas*, *Pseudoalteromonas*), Rhodobacterales (*Phaeobacter*) and Flavobacteriales (NS marine group). Within M5 bacteroidota including genera belonging to Flavobacteriales order (*Aquimarina*, Mesonia and *Tenacibaculum*) and Cytophagales order (*Pseudarcicella*) were associated with Proteobacteria (*Pseudomonas* and *Marinomonas*). The heaviest fractions (D-E) concentrated the DNA of bacteria growing only on the ^{13}C-labelled *A. sativa* vascular plant and not on ^{12}C-*S. costatum*. Modules M1 and M4 represented 19.42 and 5.83% of the nodes of the network, respectively (Fig. 6-3, Fig. S3-2) showed very significant correlations with biodegradation of TPOM including cuticular waxes (Fig. 6-5). M1 also included two Cyanobacteria (*Synechococcus* and *Prochlorococcus*), Flavobacteriales (NS marine group) and Gammaproteobacteria (*Alteromonas*, *Pseudoalteromonas*, *Marinobacter*). M4 grouped new genera belonging to Bacteroidota (*Balneola* and *Arcticiflavibacter* amongst Flavobacteriales order). Unexpectedly, none of the genera belonging to the Sphingomonadales and Rhizobiales orders that were more abundant at the end of incubation in the DE band were directly included in modules that correlate strongly with the rate of degradation of TPOM tracer compounds.

Discussion

Lipid composition of *A. sativa* leaves

Quantification of labelled lipids allowed for the detection of *A. sativa* bacterial remineralization during the incubations (TPOM model). We excluded palmitic acid, which may

be produced by bacteria growing on ^{13}C-labelled substrates, and ferulic and *p*-coumaric acids, whose volatile TMS derivatives can be lost by evaporation, during the silylation process. Moreover, the production of these two phenolic acids, during biodegradation of biopolymers (Otto et al 2005; Fazary & Ju, 2007; Xu et al. 2018), clearly compromises these results. We utilized the following labelled lipids to detect *A. sativa* remineralization: phytol, C_{24}-C_{28} alkan-1-ols, $C_{20:0}$ and $C_{22:0}$ fatty acids, sitosterol, β-amyrin and products of alkaline depolymerisation of cuticular waxes i.e. isomeric dihydroxyhexadecanoic acids (mainly 9,16- and 10,16-) and 9,10-epoxy-18-hydroxyoctadecanoic acid (Holloway & Deas 1973; Deas & Holloway1977; Kolattukudy 1980), the epoxy group of the latter being converted to the corresponding methoxyhydrins, triols, and chlorohydrins during the treatment (Marchand & Rontani 2001) (Fig. S1).

Experimental degradation of *A. sativa* lipids

Incubations were carried out under aerobic conditions, hence, the effects of autoxidative processes on TPOM degradation could not be totally excluded. Autoxidation can operate in all oxic aquatic environments (Schaich 2005) and potentially affect all unsaturated lipids (Rontani 2012; Rontani & Belt 2020). However, the decrease in concentrations of 24-ethylcholesta-3β,5α,6β–triol and 3,7,11,15-tetramethyl-hexadec-2(*Z*/*E*)-en-1,4-diols (specific autoxidation products of sitosterol and phytol, respectively; Rontani & Aubert 2005; Rontani et al. 2014), provided evidence that observed lipid decay in the incubations were microbially-mediated with no autoxidative artifact.

Examination of ^{13}C incorporation in octadec-9-enoic (oleic) acid (main fatty acid of fungi; Athenaki et al. 2017) and 13-methyltetradecanoic, hexadec-11-enoic, 2-hydroxy-13-methyltetradecanoic and 3-hydroxy-13-methyltetradecanoic acids (fatty and hydroxy acids specific to bacteria; Fautz et al. 1979; Harwood & Russell 1984; Blumenberg et al. 2005) (Figs.

3 and 4) clearly demonstrated that the primary microbes responsible for the assimilation of ^{13}C-labelled *A. sativa* were bacteria. The lack of labelled archaeol (well-known tracer of Archaebacteria; Sustar et al. 2012) during the incubation and SIP results (see Fig. 2 where Archaebacteria are in the "other" phylum) do not support the involvement of Archaebacteria in the degradation of *A. sativa*.

Enhanced bacterial degradation of some *A. sativa* lipids (phytol, C_{24}-C_{30} alkanols and cuticular waxes) in the presence of diatoms (Table 1, Fig. 1), provides possible evidence of positive priming effects (Guenet et al. 2010; Bianchi et al. 2011). However, it is interesting to note that this enhanced degradation in the presence of diatoms was not observed for C_{20} and C_{22} fatty acids and sitosterol (Table 1, Fig. 1). Interestingly, this shows that efficiency of a possible priming effect is targeted to certain compounds in vascular plants, something that will clearly help in resolving some inconsistencies in past priming studies (see Bengtsson et al. 2018; Sanches et al. 2021). In particular, this selectivity may be attributed to: (i) an increase of the biomass of specific bacteria resulting from the consumption of reactive substrates, such as algal fatty acids, amino acids and sugars (Grant & Betts 2004), or (ii) an enhanced microbial production of extracellular enzymes, able to degrade some *A. sativa* components, driven by the degradation of algal priming components (Guenet et al. 2010, Ward et al. 2016)

We posit these results are in good agreement with: (i) the strong degradation of TPOM previously observed during incubations of Rhône SPM containing a high proportion of freshwater diatoms in seawater (Bonin et al. 2019), and (ii) the increase of bacterial degradation of vascular plant material with the proportion of algal sterols, observed in SPM samples collected in the salinity gradient of the Rhône Estuary (Bonin et al. 2019). Observations of enhanced microbial respiration at the confluence of turbid and clear waters of the Amazon River revealed similar findings (Ward et al. 2019a). Thus, the incubation experiment indirectly supports previous speculations by Bonin et al. (2019), that priming may have been occurring

across similar steep turbidity and algal gradients in the Rhône Estuary. High rates of lipid decomposition are similarly observed in other dynamic settings where diverse processes occur such as newly deposited material at the estuarine and marine sediment interfaces (Canuel & Martens 1996; Sun et al. 2000), remineralization of sinking particles (Meyers & Eadie, 1992), and turbidity currents (Treignier et al. 2006). These are all environmental settings where priming effects could potentially occur (e.g. Aller & Cochran 2019), though have not necessarily been frequently observed based on experimental techniques applied to date (Bengtsson et al. 2018).

Bacteria and the assimilation of *A. sativa*

In the case of our observations of different relative abundances of some genera under different incubation conditions, we note that the addition of diatoms does not drastically modify microbial community structure. The most striking differences were observed in the lightest fraction where Gammaproteobacteria were dominant. These opportunistic copiotroph organisms took advantage of the fresh organic matter supply. In contrast, we did not observe clear modification of the biodiversity of microorganisms that assimilated ^{13}C- *A. Sativa*, whereas the biodegradation of ^{13}C-lipids was very strongly stimulated. Thus, the addition of fresh OM (diatoms) along with TPOM represents a readily available source of energy, C and nutrients for microorganisms, and a consecutive stimulation of enzymatic activities as it has generally been reported in soil (Kandeler et al. 1999; Marschner et al. 2003). The biodegradation of TPOM prokaryotic community in soils, limited by the energy available, would be activated by the addition of fresh OM, an energy source in terms of C-rich and labile molecules. This activation would lead to a strong release of extracellular enzymes and to an increase in the mineralisation of the TPOM without modifying the biodiversity of the microbial community. However, due to technical limitations, little is known about the role of the different

community members participating in TPOM biodegradation and its further assimilation. The use of isotopes enables linking the identity and function of microorganisms even in field studies (Dumont et al. 2006). In this study, we explore for the first time the stimulation of the mineralization of *A. Sativa*, as a model TPOM substrate labelled with ^{13}C, via priming with marine diatoms to better elucidate the dynamics and identity of microbial populations that actively assimilated the carbon of residue during its degradation process.

Flavobacteriales and Cytophagales were most abundant in the bacterial community that assimilated both ^{13}C-labelled *A. sativa* and ^{12}C- *S. costatum* and could have played a role in priming. After 14 days of incubation, the addition of ^{12}C- *S. costatum* led to a dominance of Bacteroidota (*Flavobacterium*, *Arenibacter* and *Taeseokella*), followed by Alphaproteobacteria (*Erythrobacter*, *Hyphomonas*) after 42 days. These different genera, in the presence of diatoms, appear to have assimilated both carbon sources, but were not included in the main modules that had the highest correlation with the rate of ^{13}C-lipids biodegradation. The assimilation of ^{13}C-*A. Sativa* by Bacteroidota was further supported with chemotaxonomy. For instance, bacteria of the Cytophagales order were characterized by a high content of iso-C_{15}, hexadec-11-enoic, 3-hydroxy-13-methyltetradecanoic and 3-hydroxy-15-methylhexadecanoic acids (McGraph et al. 1990; Nedashkovskaya et al. 2005), with the *Flavobacteria* genus dominated by iso-C_{15}, 2-hydroxy-13-methyltetradecanoic, 3-hydroxy-13-methyltetradecanoic and 3-hydroxy-15-methylhexadecanoic acids (Moss & Dees 1978; Zamora et al. 2013). The high presence of these ^{13}C-labelled acids (Table 2) confirms that bacteria belonging to the Bacteroidota phylum strongly contributed to the remineralization of *A. sativa*. Note that bacteria belonging to this phylum were able to grow on dead bacteria (O'Sullivan et al. 2002). Thus, the consumption of bacterial necromass, enriched in ^{13}C, could bias our conclusions. However, if bacterial growth on ^{13}C-labelled necromass was a significant factor, the isotopic signature of fatty acids of

Bacteroidetes would have increased at the end of the incubation, which was not observed (Table 2).

SIP results clearly showed that bacteria of the Bacteroidota phylum (more particularly Flavobacteria and Cytophaga) consumed both ^{13}C-labelled *A. sativa* and ^{12}C-algal material (Fig. 2) and thus play a key role in the priming effects. These bacteria, which are particularly common in estuaries (Crump et al. 1999; Böckelmann et al. 2000) and in the oceans (Kirchman 2002), are well known for their ability to catabolize polyaromatic substances (lignin) and sugar polymers (hemicellulose) from higher plants (Kisand et al. 2002), due to the presence of specific profiles of hydrolytic enzymes. They can also utilize lipids, proteins and DNA present in dead organisms (O'Sullivan et al. 2002). Moreover, members of the Bacteroidota phylum exhibit gliding motility and are therefore thought to live primarily on surfaces (DeLong et al. 1993, Riemann et al. 2000). Thus, they seem to be the ideal organisms to thrive as particle-attached bacteria in the estuaries (Crump et al. 1999), an attribute that has been suggested to play an important role in priming (Catalan et al. 2015). Moreover, Teeling et al (2012) previously observed that such bacteria responded first to the available substrates from dying diatoms and increased rapidly in cell numbers. As such, bacteria belonging to this phylum should thus play a key role in the production of the biomass needed for carrying out priming effects.

The part of the microbial community that primarily consumed the ^{13}C- *A. Sativa* TPOM tracer was found in the densest band. The modules showing a strong correlation with the lipid tracers are composed of the same genera as the modules identified in the intermediate density band (Flavobacteriales (NS marine group) and Gammaproteobacteria (*Alteromonas*, *Pseudoalteromonas, Marinobacter*)). Bacteria belonging to these genera seem to play a major role in the degradation and assimilation of the lipidic fraction of the TPOM. In this fraction, a significant increase in the abundance of sphingomonadales and Rhizobiales was also observed and likely contributed to the degradation of ^{13}C-*A. sativa* (Fig. 2). The lack of correlation

between the degradation of ^{13}C-labelled lipid tracers and the abundance of these bacteria suggests that these organisms mainly grew on non-lipidic ^{13}C-labelled components of *A. sativa* (e.g. sugars, proteins, lignocellulose and lignin). It is interesting to note that *Sphingomonas paucimobilis* SYK-6, which is one of the most well-characterized lignin-degrading bacteria (Masai et al. 1999), produces specific enzymes, such as β-etherases, O-demethylases, and ring fission dioxygenases, which are essential in the lignin metabolic pathway (Sonoki et al. 2002). The presence of such enzymes in Sphingomonadales makes these species particularly well adapted to the degradation of higher plant material. *Rhizobium* species, which are widely distributed in nature and are usually isolated from the plant rhizosphere (Yoon et al. 2010; Sun et al. 2013), also possess the genomic and physiological capability to metabolize lignin and lignin-like compounds (Jackson et al. 2017). Due to the simultaneous presence of lignin-oxidizing and carbohydrate-hydrolyzing genes in Rhizobiales (Jackson et al. 2017), these bacteria are also able to efficiently degrade lignocellulose. Unfortunately, ^{13}C-incorporation in fatty acids of Sphingomonadales and Rhizobiales could not be measured. Sphingomonadales are generally characterized by the presence of sphingolipids and 2-hydroxyacids (Busse et al. 1999). The 2-hydroxyacids, linked to sphingosine by amide bonds, are only very weakly hydrolyzed during the alkaline hydrolysis step employed during the treatment. The preponderance of amide-linked fatty acids is also a characteristic of Rhizobiales (Russa et al. 1995).

These results suggest an apparent priming effect that resulted from synergistic interactions between different bacterial groups, each utilizing different substrates, in contrast to priming associated with single bacterial population utilizing both algal and higher plant materials (Bianchi et al., 2015). Prior incubation studies have not identified any dominant phylogenetic group in the Bacteroidota phylum, involved in the decomposition of low and high molecular weight dissolved organic matter, further supporting the notion that diverse

assemblages and consortia drive organic matter remineralization in the ocean (Cottrell & Kirchman, 2000). Similarly, another recent study has shown that the presence of algal material in coastal waters triggers unique genomic functions associated with aromatic carbon degradation, but did not demonstrate whether one or many microbial taxa were responsible for this response (Ward et al. 2019b).

Conclusions

Incubation of ^{13}C-labelled *A. sativa* leave debris (TPOM model) in seawater (with and without amendments of the diatom *S. costatum*) with Rhône SPM as inoculum showed an enhancement of the decomposition of some *A. sativa* lipid components (phytol, *n*-alkan-1-ols and cuticular waxes) in the presence of diatoms. The lack of effect of algal amendment on the degradation of other lipids (fatty acids and sitosterol) supports an apparent selective positive priming effect. Using molecular markers, we were able to identify that bacteria of the Bacteroidota phylum played a dominant role in priming-induced TPOM degradation in estuarine waters. Priming of TPOM was carried out by a consortium of microbes (mainly *Flavobacteria* and *Cytophaga*) after consumption of labile substrates. Sphingomonadales and Rhizobiales microbes that possess enzymes needed for lignin and hemicellulose metabolism may also contribute to TPOM degradation in aquatic environments. However, in the case of this experiment their abundance was not stimulated by the presence of algal substrates.

This study provides insight into the molecular-level chemical and biological mechanisms involved in priming of TPOM degradation in estuarine environments, which is a first step in elucidating where and when priming effects occur and how relevant this process is on ecosystem to global scales. Future research should further evaluate the underlying mechanisms by which priming effects vary along salinity and river mouth-continental shelf gradients to further constrain the fate of terrigenous material in the coastal zone. Likewise, it is critical to

explore the impact of increasing coastal eutrophication on the decomposition of TPOM both as it is delivered from rivers to the sea and after being stored in coastal sediments.

Acknowledgements

This study was carried out in the framework of the project BALTOMS supported by the Labex OT-Med (through ANR-11-LABX-0061) funded by the French Government "Investissements d'Avenir" program of the French National Research Agency (ANR) through the A*MIDEX project (ANR-11-IDEX-0001-02). Thanks are due to the FEDER OCEANOMED (N° 1166-39417) for the funding of the apparatus employed. We have no conflict of interest.

References

Aller RC, Cochran JK (2019). The critical role of bioturbation for particle dynamics, priming potential, and organic C remineralization in marine sediments: local and basin scales. Front. Earth Sci. **7**: 157. doi: 10.3389/feart.2019.00157

Athenaki M, Gardeli C, Diamantopoulou P, Tchakouteu SS, Sarris D, Philippoussis A, Papanikolaou S (2017). Lipids from yeasts and fungi: physiology, production and analytical considerations. J. Appl. Microbiol. 124: 336-367. doi: 10.1111/jam.13633

Bastian M, Heymann S, Jacomy M (2009). Gephi: an open source software for exploring and manipulating networks. In Proceedings of the international AAAI conference on web and social media 3: 361-362

Bastida F, García C, Fierer N, Eldridge DJ, Bowker M A, Abades et al. (2019). Global ecological predictors of the soil priming effect. Nature Commun. 10: 1-9.

Benner R, Maccubbin AE, Hodson RE (1984). Anaerobic biodegradation of the lignin and polysaccharide components of lignocellulose and synthetic lignin by sediment microflora. Appl. Environ. Microbiol. 47: 998-1004. doi: 10.1128/aem.47.5.998-1004.1984

Bengtsson MM, Attermeyer K, Catalán N (2018). Interactive effects on organic matter processing from soils to the ocean: are priming effects relevant in aquatic ecosystem. Hydrobiologia 822: 1-17. doi: 10.1007/s10750-018-3672-2

Berner RA (1982). Burial of organic carbon and pyrite sulfur in the modern ocean: its geochemical and environmental significance. Am. J. Sci. 282. doi: 10.2475/ajs.282.4.451

Bianchi TS (2011). The role of terrestrially derived organic carbon in the coastal ocean: A changing paradigm and the priming effect. Proc. Nat. Soc. Acad. Sci. 108: 19473-19481. doi: 10.1073/pnas.1017982108

Bianchi TS, Wysocki LA, Schreiner KM, Filley TR, Corbett DR, Kolker AS (2011). Sources of terrestrial organic carbon in the Mississippi plume region: evidence for the importance of coastal marsh inputs. Aquat. Geochem. 17: 431-456. doi: 10.1007/s10498-010-9110-3

Bianchi TS, Goni M, Allison M, Chen N, McKee B (2013). Sedimentary carbon dynamics of the Atchafalaya and Mississippi River Delta system and associated margin. pp. 473-502. *In* T. S. Bianchi, M. A. Allison, and W.-J. Cai [eds.], Biogeochemical dynamics at major river-coastal interfaces: linkages with global change, Cambridge University Press.

Bianchi TS, Thornton DCO, Yvon-Lewis SA, King GM, Eglinton TI, Shields MR, Ward ND, Curtis J (2015). Positive priming of terrestrially derived dissolved organic matter in a freshwater microcosm system. Geophys. Res. Lett. 42: 5460-5467. doi: 10.1002/2015GL064765

Bianchi TS, Morrison ES (2018). Re-plumbing the earth's surface: new corridors for organismal and biogeochemical change? American Geophysical Union, Fall Meeting.

Bianchi TS, Morrison E, Barry S, Arellano AR, Feagin RA, Hinson A, Eriksson M, Allison M, Osburn CL, Oviedo-Vargas D (2018). The fate and transport of allochthonous blue carbon in divergent coastal systems, pp. 25-48. *In* L. Windham-Myers, S. Crooks, and T. G. Troxler [eds.], A blue carbon primer. CRC Press, Boca Raton. doi: 10.1201/9780429435362

Bianchi TS, Anand M, Bauch CT, Canfield DE, De Meester L, Fenne K , Groffman IPM, Pace ML, Saito M, Simpson MJ (2021) Biogeochemistry: its future role in sustainability science. Biogeosciences 18: 3005-3013. doi: 10.5194/bg-18-3005-2021

Bjordal CG (2012). Microbial degradation of waterlogged archaeological wood. J. Cult. Herit. 13: S118-S122. doi: 10.1016/j.culher.2012.02.003

Bjordal CG, Dayton PK (2020). First evidence of microbial wood degradation in the coastal waters of the Antarctic. Sci. Rep. 10: 12774. doi: 10.1038/s41598-020-68613-y

Blanchette RA (2010). Microbial degradation of wood from aquatic and terrestrial environments, pp. 179-190. In Mitchell R, McNamara CJ [eds.], Cultural heritage microbiology: fundamental studies in conservation science. ASM Press, Washington, D.C.

Blumenberg M, Seifert R, Nauhaus K, Pape T, Michaelis W (2005). In vitro study of lipid biosynthesis in an anaerobically methane-oxidizing microbial mat. Appl. Environ. Microbiol. 71: 4345–4351. doi: 10.1128/AEM.71.8.4345-4351.2005

Böckelmann U, Manz W, Neu TR, Szewzyk U (2000). Characterization of the microbial community of lotic organic aggregates (‘river snow’) in the Elbe River of Germany by cultivation and molecular methods. FEMS Microbiol. Ecol. 33: 157–170, doi: 10.1111/j.1574-6941.2000.tb00738.x

Boetius A, Lochte K (1996). Effect of organic enrichments on hydrolytic potentials and growth of bacteria in deep-sea sediments. Mar. Ecol. Progr. Ser. 140: 239-250. doi: 10.3354/meps140239

Bonin P, Prime AH, Galeron MA, Guasco S, Rontani JF (2019). Enhanced biotic degradation of terrestrial POM in an estuarine salinity gradient: interactive effects of organic matter pools and changes of bacterial communities. Aquat. Microb. Ecol. 83: 147-159. doi : 10.3354/ame01908

Bourgeois S, Pruski AM, Sun MY, Buscail R, Lantoine F, Vétion G, Rivière B, Charles F (2011). Distribution and lability of land-derived organic matter in the surface sediments of the Rhône prodelta and the adjacent shelf (Mediterranean Sea, France): a multi proxy study. Biogeosciences 8: 3107–3125. doi: 10.5194/bg-8-3107-2011

Bugg TDH, Ahmad M, Hardiman EM, Rahmanpour R (2011). Pathways for degradation of lignin in bacteria and fungi. Nat. Prod. Rep. 28**:**1883-1896. doi: 10.1039/C1NP00042J

Burdige DJ (2005). Burial of terrestrial organic matter in marine sediments: a re-assessment. Global Biogeochem. Cycles 9: GB4011. doi: 10.1029/2004GB002368

Busse HJ, Kämpfer P, Denner EBM (1999). Chemotaxonomic characterisation of *Sphingomonas*. J. Indust. Microbiol. Biotechnol. 23: 242–251. doi: 10.1038/sj.jim.2900745

Callahan BJ, McMurdie PJ, Rosen MJ, Han AW, Johnson AJA, Holmes SP (2016). DADA2: high-resolution sample inference from Illumina amplicon data. Nat. Methods 13: 581–583. doi: 10.1038/nmeth.3869

Canuel EA, Martens CS (1996). Reactivity of recently deposited organic matter: Degradation of lipid compounds near the sediment-water interface. Geochim. Cosmochim. Acta, 60: 1793-1806. doi: 10.1016/0016-7037(96)00045-2

Caporaso JG, Lauber CL, Walters WA, Berg-Lyons D, Huntley J, Fierer N, Owens SM, Betley J, Fraser L, Bauer M, Gormley N, Gilbert JA, Smith G, Knight R (2012). Ultra-high-throughput microbial community analysis on the Illumina HiSeq and MiSeq platforms. ISME J. 6: 1621–1624. doi: 10.1038/ismej.2012.8

Catalán N, Kellerman AM, Peter H, Carmona F, Tranvik LJ (2015). Absence of a priming effect on dissolved organic carbon degradation in lake water, Limnol. Oceanogr. 60: 159–168. doi: 10.1002/lno.10016

Cottrell MT, Kirchman DL (2000). Natural assemblages of marine Proteobacteria and members of the Cytophaga-Flavobacter cluster consuming low- and high- molecular-weight dissolved organic matter. Appl. Environ. Microbiol. 66: 1692–1697. doi: 10.1128/AEM.66.4.1692-1697.2000

Crump BC, Armbrust EV, Baross JA (1999). Phylogenetic analysis of particle-attached and free-living bacterial communities in the Columbia River, its estuary, and the adjacent coastal ocean. Appl. Environ. Microbiol. 65: 3192-3204. doi: 10.1128/AEM.65.7.3192-3204.1999

Deas AHB, Holloway PJ (1977). The intermolecular structure of some plant cutins, pp. 293-299. *In* Tevini M, Lichtenthaler HK [eds.], Lipids and lipid polymers in higher plants. Springer, Berlin, Heidelberg. doi: 10.1007/978-3-642-66632-2_16

de Leeuw JW, Largeau C (1993). A review of macromolecular organic compounds that comprise living organisms and their role in kerogen, coal, and petroleum formation. Org. Geochem. 11: 23–72. doi: 10.1007/978-1-4615-2890-6_2

DeLong EF, Franks DG, Alldredge AL (1993). Phylogenetic diversity of aggregate-attached vs. free-living marine bacterial assemblages. Limnol. Oceanogr. 38: 324-334. doi: 10.4319/lo.1993.38.5.0924

Fautz E, Rosenfelder G, GrotjahnL (1979). Iso-branched 2- and 3-hydroxy fatty acids as characteristic lipid constituents of some gliding bacteria. J. Bacteriol. 140: 852-858. doi: 10.1128/jb.140.3.852-858.1979

Fazary AE, Ju YH (2007). Feruloyl esterases as biotechnological tools: current and future perspectives. Acta Biochim. Biophys. Sin. 39: 911-828. doi: 10.1111/j.1745-7270.2007.00348.x

Filannino P, Bai Y, Di Cagno R, Gobbetti M, Gänzle MG (2015). Metabolism of phenolic compounds by *Lactobacillus* spp. during fermentation of cherry juice and broccoli puree. Food Microbiol. 46: 272-279. doi: 10.1016/j.fm.2014.08.018

Fujimoto YC, Chen S Szeleczky Z, Ditullio D, Sih CJ (1982). Microbial degradation of the phytosterol side chain. I. Enzymic conversion of 3-oxo-24-ethylcholest-4-en-26-oic acid into 3-oxochol-4-en-24-oic acid and androst-4-ene-3,17-dione. J. Am. Chem. Soc. 104: 4718–4720. doi: 10.1021/ja00381a055

Galeron MA, Amiraux R, Charriere B, Radakovitch O, Raimbault P, Garcia N, Lagadec V, Vaultier F, Rontani JF (2015). Seasonal survey of the composition and degradation state of particulate organic matter in the Rhône River using lipid tracers. Biogeosciences 12: 1431–1446. doi: 10.5194/bg-12-1431-2015

Garel M, Bonin P, Martini S, Guasco S, Roumagnac M, Bhairy N, Armougom F, Tamburini C (2019). Pressure-retaining sampler and high-pressure systems to study deep-sea microbes under in situ conditions. Front. Microbiol. 10: 453. doi: 10.3389/fmicb.2019.00453

Grant RJ, Betts BW (2004). Mineral and carbon usage of two synthetic pyrethroid degrading bacterial isolates. J. Appl. Microbiol. 97: 656-662. doi: 10.1111/j.1365-2672.2004.02358.x

Guenet B, Camino-Serrano M, Ciais P, Tifafi M, Maignan F, Soong JL, Janssens IA (2010). Impact of priming on global soil carbon stocks. Global Change Biol. 24: 1873-1883. doi: 10.1111/gcb.14069

Guenet B, Danger M, Harrault L, Allard B, Jauset-Alcala M, Bardoux G, Benest D, Abbadie L, Lacroix G (2014). Fast mineralization of land-born C in inland waters: first experimental evidence of aquatic priming effect. Hydrobiologia 721: 35–44. doi.org/10.1007/s10750-013-1635-1

Harwood JL, Russell NJ (1984). Major lipid types in plants and micro-organisms, pp. 7-34. *In* Harwood JL, Russell NJ [eds.], Lipids in plants and microbes. Springer, Dordrecht. doi: 10.1007/978-94-011-5989-0-3

Hedges JI, Keil RG (1995). Sedimentary organic matter preservation: an assessment and speculative synthesis. Mar. Chem. 49: 81-115. doi.org/10.1016/0304-4203(95)00008-F

Hedges JI, Keil RG, Benner R (1997). What happens to terrestrial organic matter in the ocean? Org. Geochem. 27: 195-212. doi: 10.1016/S0146-6380(97)00066-1

Hedges JI (2002). Sedimentary organic matter preservation and atmospheric O_2 regulation, pp. 105-123. *In* A. Gianguzza, E. Pelizzetti, S. Sammartano [eds.], Chemistry of marine water and sediments. Environmental Science. Springer, Berlin, Heidelberg. doi: 10.1007/978-3-662-04935-8_4

Holloway PJ, Deas AHB (1973). Epoxyoctadecanoic acids in plant cutins and suberins. Phytochemistry 12: 1721-1735. doi: 10.1016/0031-9422(73)80393-0

Jackson CA, Couger MB, Prabhakaran M, Ramachandriya KD, Canaan P, Fathepure BZ (2017). Isolation and characterization of *Rhizobium* sp. strain YS-1r that degrades lignin in plant biomass. J. Appl. Microbiol. 122: 940-952. doi: 10.1111/jam.13401

Jeffries TW (1991). Biodegradation of lignin-carbohydrate complexes, pp. 163-176. *In* Ratledge C [eds.], Physiology of biodegradative microorganisms. Springer, Dordrecht. doi: 10.1007/978-94-011-3452-1_7

Jones EBG, Irvine J (1971). Role of fungi in the deterioration of wood in the sea. Inst. Wood Sci. J. 31-43.

Karlsson ES, Charkin A, Dudarev O, Semiletov I, Vonk JE, Sánchez-García L, Andersson A. Gustafsson Ö (2011). Carbon isotopes and lipid biomarker investigation of sources, transport and degradation of terrestrial organic matter in the Buor-Khaya Bay, SE Laptev Sea. Biogeosciences 8: 1865–1879. doi: 10.5194/bg-8-1865-2011

Kirchman DL (2002). The ecology of *Cytophaga-Flavobacteria* in aquatic environments. FEMS Microbiol. Ecol. 39: 91-100. doi: 10.1111/j.1574-6941.2002.tb00910.x

Kisand V, Cuadros R, Wikner J (2002). Phylogeny of culturable estuarine bacteria catabolizing riverine organic matter in the Northern Baltic Sea. Appl. Environ. Microbiol. 68: 379–388. doi: 10.1128/AEM.68.1.379–388.2002

Kolattukudy PE (1980). Biopolyester membranes of plants: cutin and suberin. Science 208: 990-1000. doi: 10.1126/science.208.4447.990

Kondo T, Mizuno K, Kato T (1990). Cell wall-bound *p*-coumaric and ferulic acids in Italian ryegrass. Canadian J. Plant Sci. 71: 495-499. doi: 10.4141/cjps90-058

Kuzyakov Y, Friedel JK, Stahr K (2000). Review of mechanisms and quantification of priming effects. Soil Biol. Biochem. 32: 1485-1498. doi: 10.1016/S0038-0717(00)00084-5

Lecornu J, Michel J (1986). L'étude d'impact de la protection contre les crues du Rhône des plaines de la région de Brangues. Société hydrotechnique de France. XIXe Journées de l'Hydraulique Paris, 9-11 sept.

Liu C, Cui Y, Li X, Yao M (2021). Microeco: an R package for data mining in microbial community ecology. FEMS microbiology ecology, 97: 2 fiaa255.

Lueders T, Manefield M, Friedrich MW (2003). Enhanced sensitivity of DNA- and rRNA-based stable isotope probing by fractionation and quantitative analysis of isopycnic centrifugation gradients. Environ. Microbiol. 6: 73–8. doi: 10.1046/j.1462-2920.2003.00536.x

Marchand D, Rontani JF (2001). Characterisation of photo-oxidation and autoxidation products of phytoplanktonic monounsaturated fatty acids in marine particulate matter and recent sediments. Org. Geochem. 32: 287–304. doi: 10.1016/S0146-6380(00)00175-3

Masai E, Katayama Y, Nishikawa S, Fukuda M (1999). Characterization of *Sphingomonas paucimobilis* SYK-6 genes involved in degradation of lignin-related compounds. J. Ind. Microbiol. Biotech. 23: 364–373. doi: 10.1038/sj.jim.2900747

McGraph CF, Moss CW, Burchard PR (1990). Effect of temperature shifts on gliding motility, adhesion, and fatty acid composition of *Cytophaga* sp. Strain U67. J. Bacteriol. 172: 1978-1982. doi: 10.1128/jb.172.4.1978-1982.1990

McMurdie PJ, Holmes S (2013). phyloseq: an R package for reproducible interactive analysis and graphics of microbiome census data. Plos One 8: e61217. doi: 10.1371/journal.pone.0061217

Meyers PA, Eadie PJ (1993). Sources, degradation and recycling of organic matter associated with sinking particles in Lake Michigan. Org. Geochem. 20: 47-56. doi: 10.1016/0146-6380(93)90080-U

Moss CW, Dees SB (1978). Cellular fatty acids of *Flavobacterium meningosepticum* and *Flavobacterium* species group IIb. J. Clinic. Microbiol. 8: 772-774. doi: 10.1128/jcm.8.6.772-774.1978

Mouzouras R (1989). Soft rot decay of wood by marine microfungi. J. Inst. Wood Sci. 11: 193-201.

Multari S, Marsol-Vall A, Keskitalo M, Yang B, Suomela JP (2018). Effects of different drying temperatures on the content of phenolic compounds and carotenoids in quinoa seeds (*Chenopodium quinoa*) from Finland. J. Food Compos. Anal. 72: 75-82. doi: 10.1016/j.jfca.2018.06.008

Nedashkovskaya OI, Kim DB, Lysenko AM, Frolova GM, Mikhailov VV, Lee KH, Bae KS (2005). Description of *Aquimarina muelleri* gen. nov., sp. nov., and proposal of the reclassification of [Cytophaga] *latercula Lewin* 1969 as *Stanierella latercula* gen. nov., comb. nov. Intern. J. Syst. Evol. Microbiol. 55: 225-229. doi: 10.1099/ijs.0.63349-0

Neufeld JD, Vohra J, Dumont MG, Lueders T, Manefield M, Friedrich MW, Murrell JC (2007). DNA stable-isotope probing. Nat. Prot., 2: 860-866. doi: 10.1038/nprot.2007.109

Newton RJ, Jones SE, Eiler A, McMahon KD, Bertilsson S (2011). A guide to the natural history of freshwater lake bacteria. Microbiol. Mol. Biol. Rev. 75: 14-49. doi: 10.1128/MMBR.00028-10

Obernosterer I, Catala P, Reinthaler T, Herndl GJ, Lebaron P (2005). Enhanced heterotrophic activity in the surface microlayer of the Mediterranean Sea. Aquat. Microbiol. Ecol. 39: 293-302. doi: 10.3354/ame039293

O'Sullivan LA, Weightman AJ, Fry JC (2002). New degenerate *Cytophaga-Flexibacter-Bacteroides*-specific 16S ribosomal DNA-targeted oligonucleotide probes reveal high bacterial diversity in river Taff epilithon. Appl. Environ. Microbiol. 68: 201-210. doi: 10.1128/AEM.68.1.201-210.2002

Otto A, Simoneit BRT, Rembe WC (2005). Conifer and angiosperm biomarkers in clay sediments and fossil plants from the Miocene Clarkia Formation, Idaho, USA. Org. Geochem. 36: 907-922. doi: 10.1016/j.orggeochem.2004.12.004

Parnas H (1976). A theoretical explanation of the priming effect based on microbial growth with two limiting substrates. Soil Biol. Biochem. 8: 139-144. doi: 10.1016/0038-0717(76)90079-1

Pointing SB, Hyde KD (2000). Lignocellulose-degrading marine fungi. Biofouling 15: 221-229. doi: 10.1080/08927010009386312

Quast C, Pruesse E, Yilmaz P, Gerken J, Schweer T, Yarza P, Peplies J, Glöckner FO (2012). The SILVA ribosomal RNA gene database project: improved data processing and web-based tools. Nucl. Acids Res. 41: D590-D596. doi: 10.1093/nar/gks1219

Riemann L, Steward GF, Azam F (2000). Dynamics of bacterial community composition and activity during a mesocosm diatom bloom. Appl. Environ. Microbiol. 66: 578-587. doi: 10.1128/AEM.66.2.578-587.2000

Rontani JF, Aubert C (2005). Characterization of isomeric allylic diols resulting from chlorophyll phytyl side chain photo- and autoxidation by electron ionization gas chromatography/mass spectrometry. Rapid Commun. Mass Spectrom. 19: 637–646. doi.org/10.1002/rcm.1835

Rontani JF (2012). Photo-and free radical-mediated oxidation of lipid components during the senescence of phototrophic organisms, pp. 3–31. *In* T. Nagata, [ed.], Senescence. Intech, Rijeka.

Rontani JF, Charrière B, Sempéré R, Doxaran D, Vaultier F, Vonk JE, Volkman JK (2014). Degradation of sterols and terrigenous organic matter in waters of the Mackenzie Shelf, Canadian Arctic. Org. Geochem. 75: 61–73. doi: 10.1016/j.orggeochem.2014.06.002

Rontani JF, Belt ST (2020). Photo- and autoxidation of unsaturated algal lipids in the marine environment: An overview of processes, their potential tracers, and limitations. Org. Geochem. 139: 103941. doi: 10.1016/j.orggeochem.2019.103941

Russa R, Urbanik-Sypniewska T, Lindström K, Mayer H (1995). Chemical characterization of two lipopolysaccharide species isolated from *Rhizobium loti* NZP2213. Arch. Microbiol. 163: 345–351. doi: 10.1007/BF00404207

Sanches JF, Guenet B, dos Anjos N, Marino C, de Assis Esteves F (2021). Exploring the drivers controlling the priming effect and its magnitude in aquatic systems. JGR Biogeosciences 126(8): e2020JG006201. doi: 10.1029/2020JG006201

Scalbert A, Monties B, Lallemand JY, Guittet E, Rolando C (1985). Ether linkage between phenolic acids and lignin fractions from wheat straw. Phytochemistry 24: 1359-1362. doi: 10.1016/S0031-9422(00)81133-4

Schaich KM (2005). Lipid Oxidation: Theoretical Aspects, pp. 269–355. *In* F. Shahidi, [ed.], Bailey's industrial oil and fat products. John Wiley & Sons, Chichester. doi: 10.1002/047167849X.bio067

Singh B, Singh JP, Kaur A, Singh N (2018). Phenolic composition and antioxidant potential of grain legume seeds: A review. Food Res. Intern. 101: 1-16. doi: 10.1016/j.foodres.2017.09.026

Sonoki T, Iimura Y, Masai E, Kajita S, Katayama Y (2002). Specific degradation of β-aryl ether linkage in synthetic lignin (dehydrogenative polymerizate) by bacterial enzymes of *Sphingomonas paucimobilis* SYK-6 produced in recombinant *Escherichia coli*. J. Wood Sci. 48: 429–433. doi: 10.1007/BF00770705

Steen AD, Quigley LNM, Buchan A (2016). Evidence for the priming effect in a planktonic estuarine microbial community. Front. Mar. Sci. 3: 6. doi: 10.3389/fmars.2016.00006

Sun MY, Shi W, Lee RF (2000). Lipid-degrading enzyme activities associated with distribution and degradation of fatty acids in the mixing zone of Altamaha estuarine sediments. Org. Geochem. 31: 889-902. doi: 10.1016/S0146-6380(00)00051-6

Sun MY, He Y, Xiao Q, Ye R, Tian Y (2013). Isolation, characterization, and antimicrobial activity of endophytic bacteria from *Polygonum cuspidatum*. African J. Microbiol. Res. 7: 1496-1504.

Sustar V, Zelko J, Lopalco P, Lobasso S, Ota A, Ulrih NP, Corcelli A, Kralj-Iglic V (2012). Morphology, biophysical properties and protein-mediated fusion of archaeosomes. Plos One **7**: e39401. doi: 10.1371/journal.pone.0039401

Teeling H, Fuchs BM, Becher D, Klockow C, Gardebrecht A, Bennke CM, Amann R (2012). Substrate-controlled succession of marine bacterioplankton populations induced by a phytoplankton bloom. Science 336: 608-611. doi: 10.1126/science.1218344

Treignier C, Derenne S, Saliot A (2006). Terrestrial and marine *n*-alcohol inputs and degradation processes relating to a sudden turbidity current in the Zaire canyon. Org. Geochem. 37: 1170-1184. doi: 10.1016/j.orggeochem.2006.03.010

Triebl A, Wenk MR (2018). Analytical considerations of stable isotope labelling in lipidomics. Biomolecules 8: 151. doi: 10.3390/biom8040151

Vonk JE, Sanchez-Garcia L, Semiletov IP, Dudarev OV,. Eglinton TI, Andersson A, Gustafsson Ö (2010). Molecular and radiocarbon constraints on sources and degradation of terrestrial organic carbon along the Kolyma paleoriver transect, East Siberian Sea. Biogeosciences 7: 3153–3166. doi: 10.5194/bg-7-3153-2010

Ward ND, Bianchi TS, Sawakuchi HO, Gagne-Maynard W, Cunha AC, Brito DC, Neu V, de Matos A, da Silva VR, Krusche AV, Richey JE, Keil RG (2016). The reactivity of plant-derived organic matter and the potential importance of priming effects along the lower Amazon River. JGR Biogeosciences 121: 1522-1539. doi: 10.1002/2016JG003342

Ward ND, Bianchi TS, Medeiros PM, Seidel M, Richey JE, Keil RG, Sawakuchi HO (2017). Where carbon goes when water flows: carbon cycling across the aquatic continuum. Front. Mar. Sci. 4: 7. doi: 10.3389/fmars.2017.00007

Ward ND, Sawakuchi HO, Richey JE, Keil RG, Bianchi TS (2019a). Enhanced aquatic respiration rates associated with mixing of clearwater tributary and turbid Amazon River waters. Front. Earth Sci. 7: 101. doi: 10.3389/feart.2019.00101

Ward ND, Morrison E, Liu Y, Rivas-Ubach A, Osborne TZ, Ogram A, Bianchi TS (2019b). Marine microbial responses related to wetland carbon mobilization in the coastal zone. Limnol. Oceanogr. Lett. 4: 25-33. doi: 10.1002/lol2.10101

Ward ND, Megonigal JP, Bond-Lamberty B, Bailey VL, Butman D, Canuel EA, Windham-Myers L (2020). Representing the Function and Sensitivity of Coastal Interfaces in Earth System Models. Nat. Commun. 11: 2458. doi: 10.1038/s41467-020-16236-2

Xu R, Zhang K, Liu P, Han H, Zhao S, Kakade A, Khan A, Du D, Li X (2018). Lignin depolymerization and utilization by bacteria. Biores. Technol. 269: 557-566. doi: 10.1016/j.biortech.2018.08.118

Yoon JH, Kang SJ, Yi HS, Oh TK, Ryu CM (2010). *Rhizobium soli* sp. nov., isolated from soil. Intern. J. Syst. Evol. Microbiol. 60: 1387–1393. doi: 10.1099/ijs.0.013094-0

Zamora L, Vela AI, Sánchez-Porro C, Palacios MA, Domínguez L, Moore ERB, Ventosa A, Fernández-Garayzábal JE (2013). Characterization of flavobacteria possibly associated with fish and fish farm environment. Description of three novel *Flavobacterium* species: *Flavobacterium collinsii* sp. nov., *Flavobacterium branchiarum* sp. nov., and *Flavobacterium branchiicola* sp. nov. Aquaculture 416–417: 346-353. doi: 10.1016/j.aquaculture.2013.09.019

FIGURE CAPTIONS

Fig. 1. Degradation of lipid components of ^{13}C-labelled *A. sativa* during the incubations.

Fig. 2. Taxonomic affiliation of the 5 most abundant phyla (A), amongst the class of Gammaproteobacteria (B), amongst the class of Alphaproteobacteria (C) and amongst Bacteroidota (D) obtained from the 16*S* rRNA gene (DNA) sequences at different sampling times during the incubation. The group "Other" contains all phyla with relative abundance lower than 1% of the total community.

Fig. 3. TOF MS mass spectra of octadec-9-enoic (A), 13-methyltetradecanoic (B) and hexadec-11-enoic (C) acid TMS derivatives at the end of the incubation.

Fig. 4. TOF MS mass spectra of 2-hydroxy-13-methyltetradecanoic acid (A) and 3-hydroxy-13-methyltetradecanoic acid TMS derivatives at the end of the incubation.

Fig. 5. Heatmap showing the normalized abundance (Z-score by row) of differentially abundant genera belonging to Bacteriodota and Proteobacteria (alpha and gamma) phyla. Boxplot representing the distribution of Log-transformed relative abundances in different samples.

Fig. 6. Co-occurrence network based on correlation analysis. Each node denotes a microbial genera. Node size is proportional to the degree (that is, the number of links from this node to any other node) and node color denotes taxonomic classification. Edge lines between nodes represent significant co-occurrences relationships. Edge size indicates the strength of Spearman correlation among nodes. 1, 2 and 3 represent co-occurrence network of A, BC and CE bands, respectively. 4 and 5 show the correlations between module eigengenes and environmental traits in the core community network. The color of each plot indicates the correlation between corresponding module eigengenes and environmental trait. Red color means highly positive correlation and green color means highly negative correlation. Pearson correlation matrix (Fig. 6-4; 6-5) between module and environmental parameters. The color indicates the correlation

coefficient intensity (rho), the p-values are indicated in the plots and in its significance with (*): P > 0.05 ; * : p ≤ 0.05 ; ** ≤ 0.01; *** ≤ 0.001.

Supplementary material

Fig. S1. Total ion current chromatogram of the total lipid extract of *A. sativa*.

Fig. S2. Taxonomic affiliation of the 5 most abundant phyla (A), amongst the class of Gammaproteobacteria (B), amongst the class of Alphaproteobacteria (C) and amongst Bacteroidota (D) obtained from the 16*S* rRNA gene (DNA) sequences at different sampling times during the incubation without *S. costatum* as cosubstrate. The group "Other" contains all phyla with relative abundance lower than 1% of the total community.

Fig. S3. Same network as in Figure 6. Modules significantly related to environmental parameters are colored.

Table S1. Data quality trimming and alpha diversity indices.

Table 1
Degradation of ^{13}C labelled *A. sativa* components during the different incubations.

Compounds	Incubation time (d)					
	0	7	15	28	42	42 (without diatoms)
Eicosanoic acid[b]	342.1 ± 110.4	131.9 ± 28.7	109.4 ± 34.4	86.8 ± 34.3	89.6 ± 11.1	112.8 ± 23.2
Docosanoic acid[b]	223.9 ± 78.9	114.6 ± 29.4	103.4 ± 35.3	88.8 ± 44.0	84.4 ± 6.3	104.7 ± 23.1
Phytol[a]	1.4 ± 0.2	0.9 ± 0.3	0.4 ± 0.2	0.6 ± 0.1	0.4 ± 0.2	1.2 ± 0.3
Tetracosan-1-ol[b]	34.8 ± 7.8	28.5 ± 9.0	22.3 ± 4.0	19.0 ± 6.9	13.9 ± 2.3	30.6 ± 6.0
Hexacosan-1-ol[a]	1.1 ± 0.2	0.8 ± 0.5	0.6 ± 0.2	0.4 ± 2.2	0.2 ± 0.1	0.8 ± 0.1
Octacosan-1-ol[b]	263.3 ± 56.6	168.9 ± 90.0	154.8 ± 65.5	112.0 ± 70.8	107.3 ± 42.7	167.6 ± 37.7
9,16- and 10,16-dihydroxyhexadecanoic acids[a]	3.2 ± 0.5	2.7 ± 0.6	2.5 ± 0.3	1.6 ± 0.4	1.3 ± 0.6	2.0 ± 0.9
9,10-Epoxy-18-hydroxyoctadecanoic acid[a]	15.5 ± 1.7	15.0 ± 4.6	10.2 ± 2.3	6.8 ± 2.3	4.6 ± 3.1	8.0 ± 2.4
Cuticular waxes[c]	18.7 ± 1.4	17.7 ± 5.1	12.7 ± 2.0	8.4 ± 2.7	5.9 ± 3.7	10.0 ± 2.1
Sitosterol[b]	193.0 ± 34.0	163.9 ± 57.2	87.0 ± 41.2	92.3 ± 25.6	63.1 ± 18.7	57.9 ± 20.1
β-Amyrin[b]	5.2 ± 1.2	6.3 ± 1.1	5.8 ± 2.4	5.7 ± 1.1	5.5 ± 1.2	5.6 ± 0.5

[a] Amount/flask (µg)
[b] Amount/flask (ng)
[c] (Isomeric dihydroxyhexadecanoic acids + 9,10-epoxy-18-hydroxyoctadecanoic acid)

Table 2
^{13}C incorporation (%)[a] in the main fatty acids during the incubation with algal cosubstrate.

Fatty acids	Initial time	Incubation for 28 days	Incubation for 42 days
Dodecanoic acid	6.0 ± 1.0	**42.3 ± 5.9**	9.4 ± 3.8
Tetradecanoic acid	7.6 ± 0.6	9.4 ± 1.6	7.0 ± 0.8
Hexadecanoic acid	6.4 ± 1.1	3.9 ± 0.6	4.1 ± 0.7
Octadecanoic acid	9.5 ± 1.0	2.3 ± 0.1	2.7 ± 0.1
12-Methyltridecanoic acid (iso C_{14})	nd[b]	**37.3 ± 4.3**	**39.0 ± 3.4**
13-Methyltetradecanoic acid (iso C_{15})	1.9 ± 0.6	**64.8 ± 7.9**	**64.5 ± 1.1**
12-Methyltetradecanoic acid (anteiso C_{15})	0.9 ± 0.3	20.1 ± 3.4	22.3 ± 2.4
Hexadec-9-enoic acid	3.6 ± 0.2	**35.0 ± 4.6**	**26.4 ± 1.5**
Hexadec-11-enoic acid	nd	**80.2 ± 3.6**	**78.5 ± 2.4**
Octadec-9-enoic acid	14.1 ± 1.4	7.0 ± 1.5	11.0 ± 2.0
Octadec-11-enoic acid	6.6 ± 0.8	**34.6 ± 8.0**	**29.2 ± 1.9**
3-Hydroxydecanoic acid	nd	24.1 ± 2.6	19.8 ± 6.7
3-Hydroxytetradecanoic acid	10.0 ± 3.0	14.7 ± 2.4	7.3 ± 0.8
3-Hydroxy-13-methyltetradecanoic acid	nd	**69.6 ± 4.9**	**61.3 ± 2.0**
3-Hydroxyhexadecanoic acid	7.7 ± 1.5	19.4 ± 1.6	15.3 ± 1.1
3-Hydroxy-15-methylhexadecanoic acid	nd	**58.9 ± 6.6**	**56.3 ± 1.8**
2-Hydroxy-13-methyltetradecanoic acid	3.4 ± 1.1	**72.4 ± 7.6**	**65.9 ± 2.0**

[a] After correction for natural ^{13}C abundance.
[b] Not detected

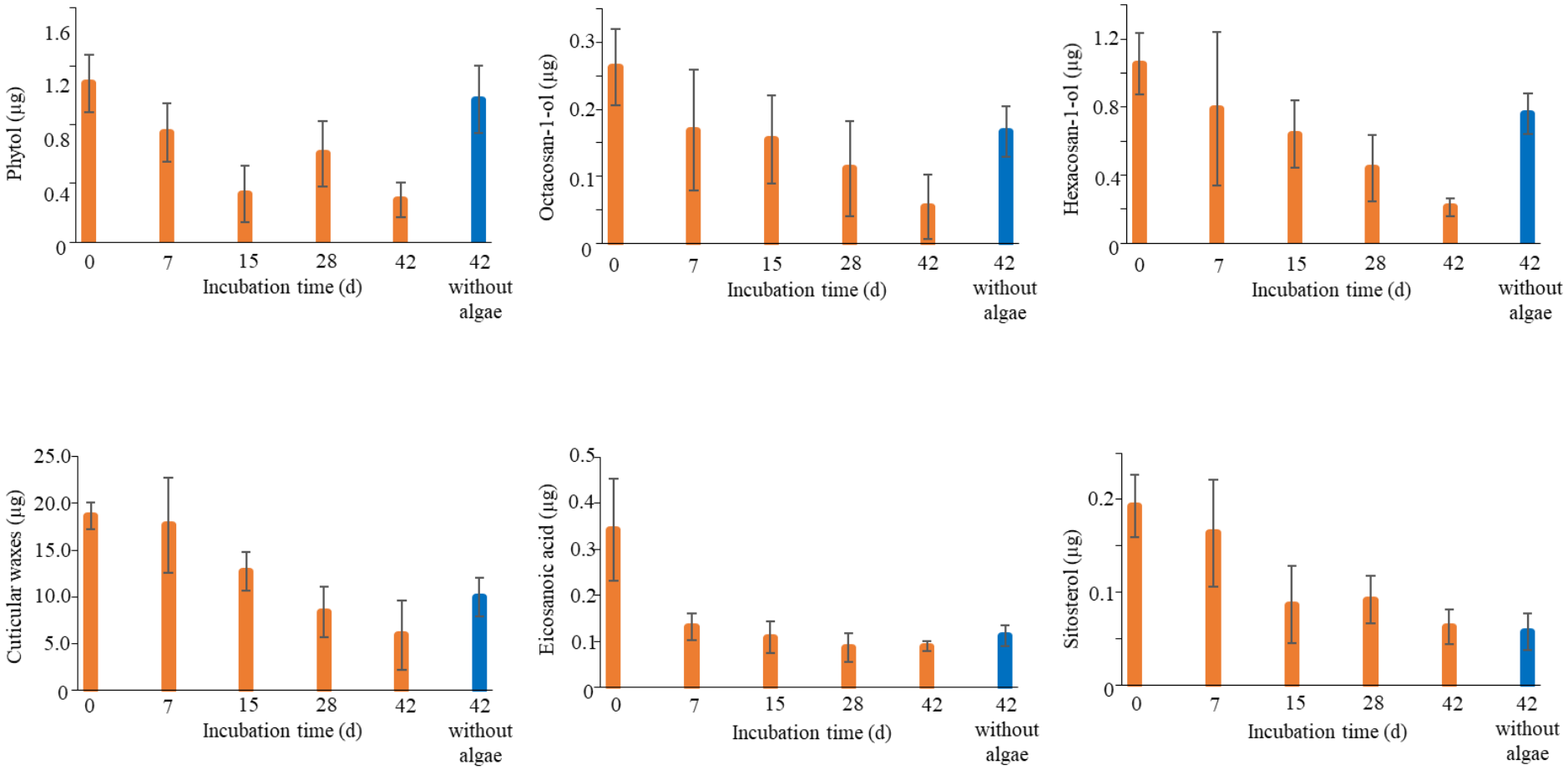

Fig. 1 : Degradation of lipid components of ^{13}C-labelled *A. sativa* during the incubations.

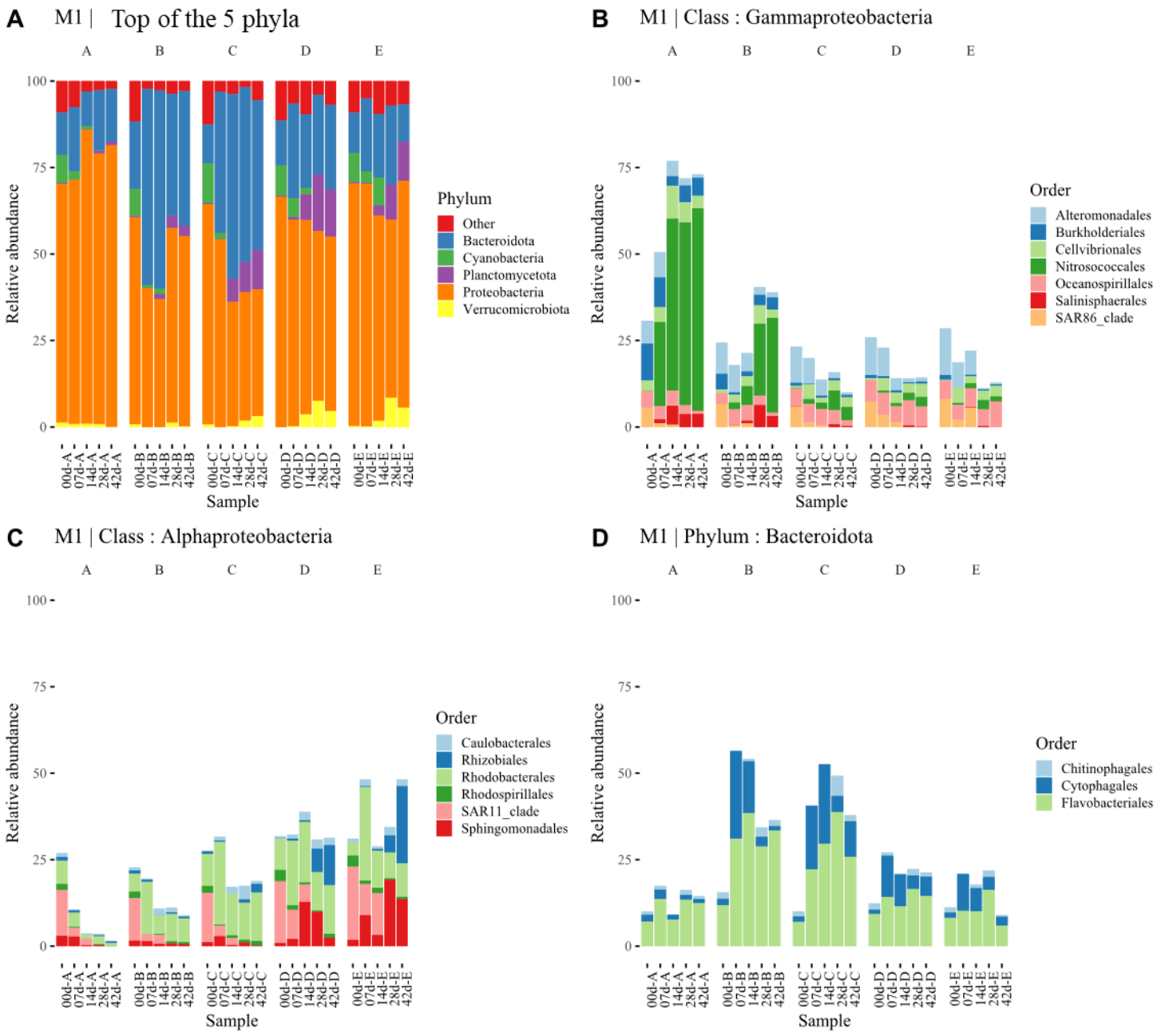

Fig. 2 : Taxonomic affiliation of the 5 most abundant phyla (A), amongst the class of Gammaproteobacteria (B), amongst the class of Alphaproteobacteria (C) and amongst Bacteroidota (D) obtained from the 16S rRNA gene (DNA) sequences at different sampling times. The group "Other" contains all phyla with relative abundance lower than 1% of the total community.

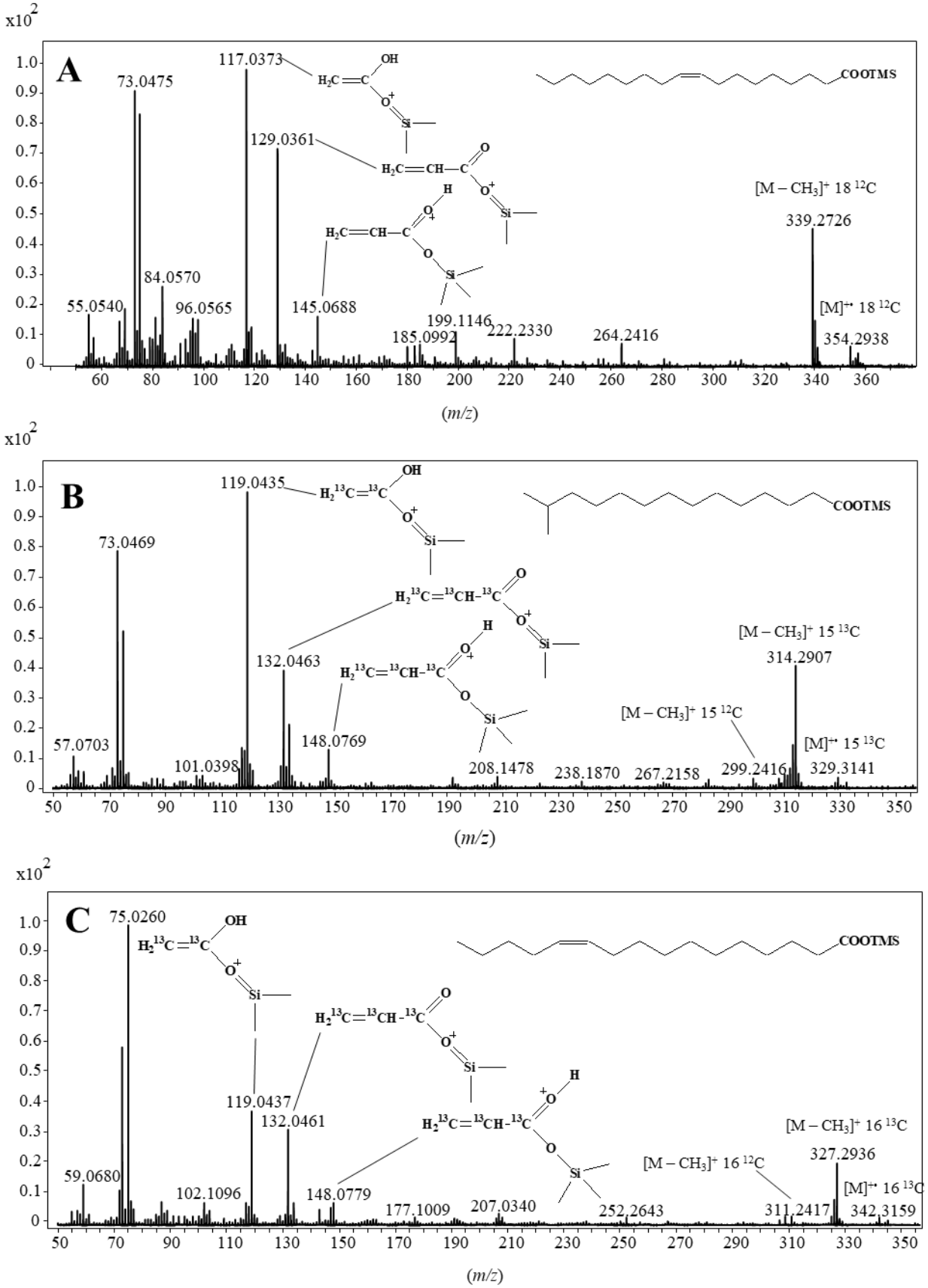

Fig, 3: TOF MS mass spectra of octadec-9-enoic (A), 13-methyltetradecanoic (B) and hexadec-11-enoic (C) acid TMS derivatives at the end of the incubation.

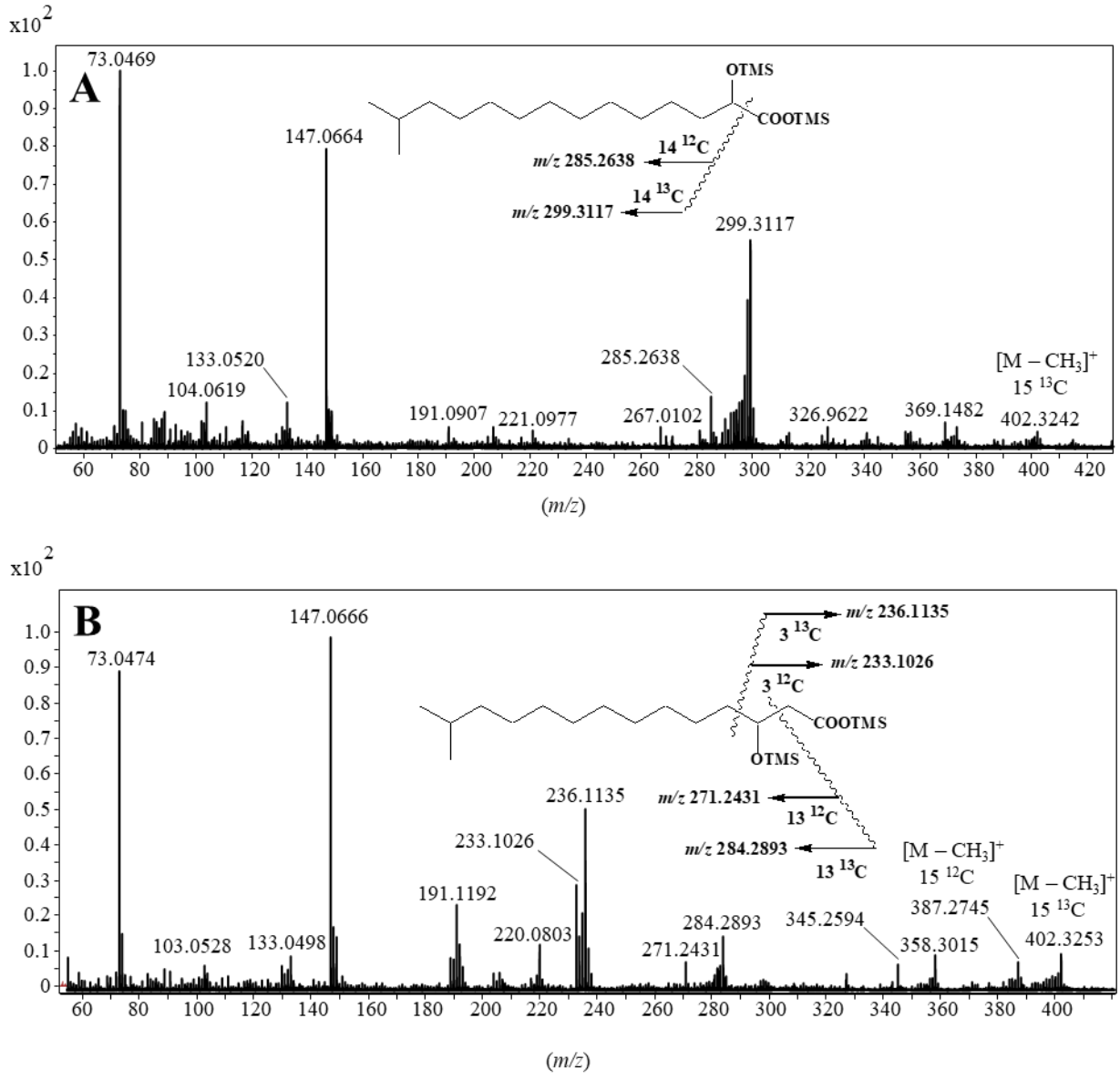

Fig. 4 : TOF MS mass spectra of 2-hydroxy-13-methyltetradecanoic acid (A) and 3-hydroxy-13-methyltetradecanoic acid TMS derivatives at the end of the incubation.

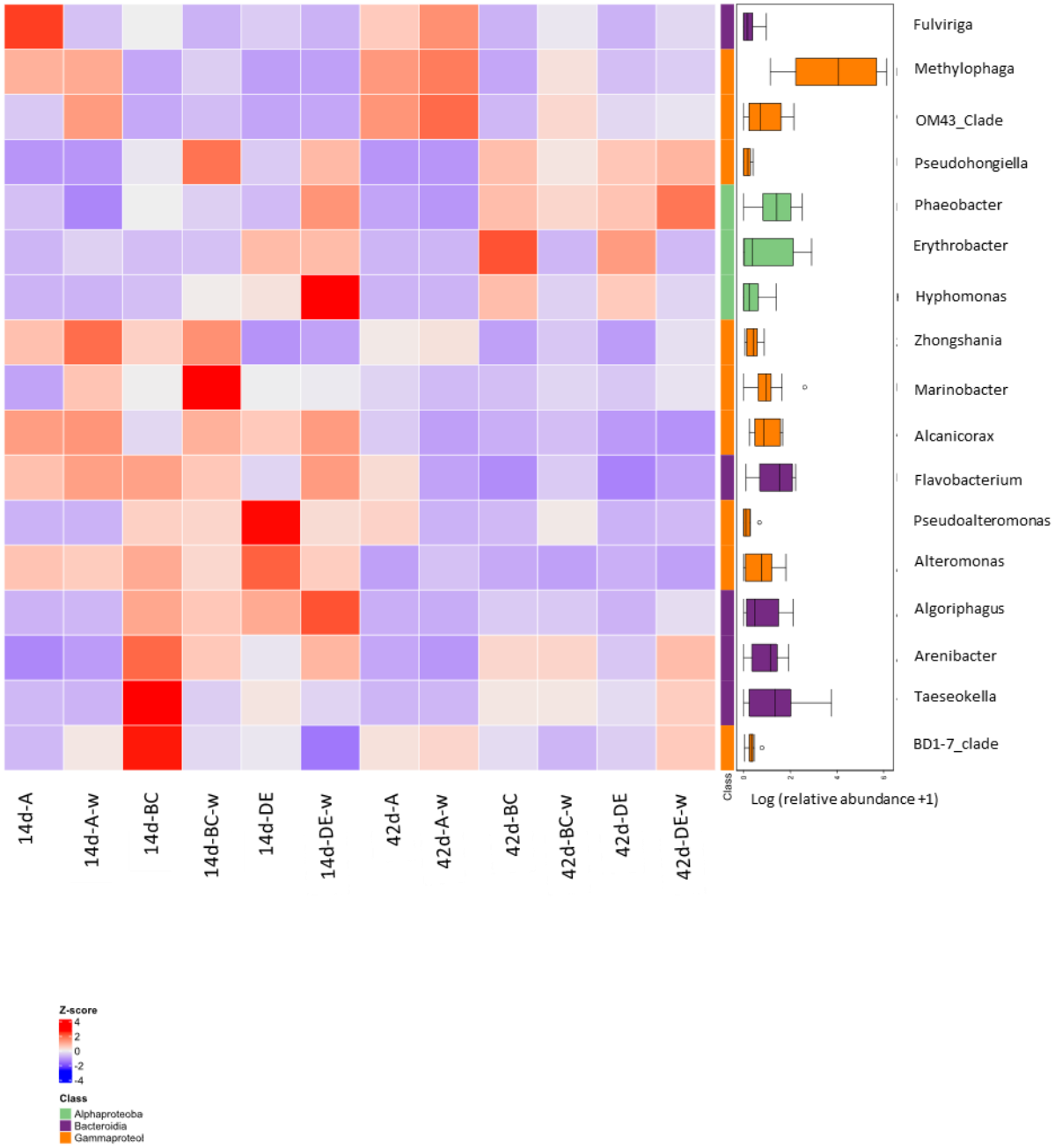

Fig. 5 : Heatmap showing the normalized abundance (Z-score by row) of differentially abundant genera belonging to Bacteriodota and Proteobacteria (alpha and gamma) phyla. Boxplot representing the distribution of Log-transformed relative abundances in different samples.

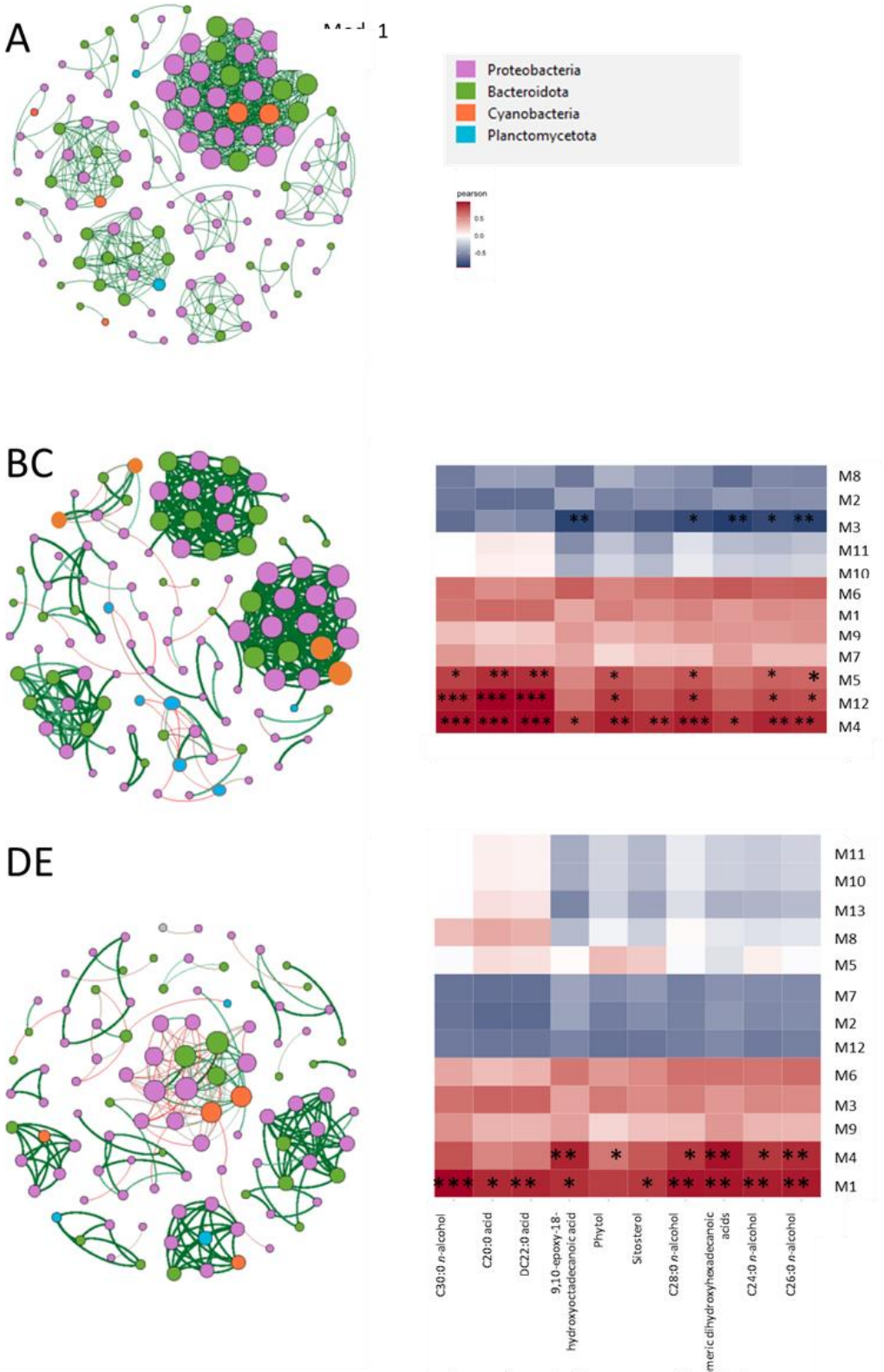

Fig. 6. Co-occurrence network based on correlation analysis. Each node denotes a microbial genera. Node size is proportional to the degree (that is, the number of links from this node to any other node) and node color denotes taxonomic classification. Edge lines between nodes represent significant co-occurrences relationships. Edge size indicates the strength of Spearman correlation among nodes. 1, 2 and 3 represent co-occurrence network of A, BC and CE bands, respectively. 4 and 5 show the correlations between module eigengenes and environmental traits in the core community network. The color of each plot indicates the correlation between corresponding module eigengenes and environmental trait. Red color means highly positive correlation and green color means highly negative correlation. Pearson correlation matrix (Fig. 6-4; 6-5) between module and environmental parameters. The color indicates the correlation coefficient intensity (rho), the p-values are indicated in the plots and in its significance with (*): P > 0.05 ; * : p ≤ 0.05 ; ** ≤ 0.01; *** ≤ 0.001.

Table S1 :

Description	imput	filtered	denoised	merged	nonchimeric	Final_retained (%)	Observed	Chao1
M1-0d-A	47338	26210	23002	16824	15379	64,98	340	345,25
M1-0d-B	49820	34337	31942	25311	20483	82,23	430	443,54
M1-0d-C	59977	40140	38929	33603	23512	78,40	359	360,65
M1-0d-D	28930	18737	17838	15016	12910	89,25	253	253,10
M1-0d-E	20273	13266	12422	10471	8830	87,11	208	208,00
M1-7d-A	54438	31293	27377	21557	17156	63,03	257	257,59
M1-7d-B	53136	35595	33583	30788	20310	76,45	202	210,25
M1-7d-C	33761	23741	22348	20433	14536	86,11	191	194,11
M1-7d-D	59192	26155	24516	20994	16275	54,99	266	269,11
M1-7d-E	44943	30690	29405	27053	18960	84,37	243	245,57
M1-14d-A	18642	12703	10762	9271	7265	77,94	95	95,00
M1-14d-B	42673	28965	26847	24141	16903	79,22	216	219,00
M1-14d-C	16057	11185	10368	9214	6752	84,10	100	100,00
M1-14d-D	54720	36133	34592	31976	21429	78,32	281	293,36
M1-14d-E	35746	25079	23855	20059	17204	96,26	321	324,06
M1-28d-A	88709	58055	55889	52336	47531	107,16	353	395,37
M1-28d-B	51938	42946	41194	38127	35123	135,25	340	366,00
M1-28d-C	64600	51356	49443	44884	36756	113,80	247	258,50
M1-28d-D	46563	38950	37477	34658	32376	139,06	268	293,55
M1-28d-E	44619	34745	32997	29955	19743	88,50	218	218,17
M1-42d-A	45136	34788	31804	28158	18984	84,12	135	138,33
M1-42d-B	78296	51417	48674	43957	22562	57,63	186	187,75
M1-42d-C	49959	38214	36506	33761	19989	80,02	232	232,00
M1-42d-D	49696	37648	35735	33139	21077	84,82	233	233,00
M1-42d-E	68401	50097	48324	44042	23644	69,13	211	211,75
M2-0d-B	41658	32500	27028	21284	16074	77,17	264	265,75
M2-0d-C	38269	29233	25001	20047	16097	84,13	283	287,00
M2-0d-D	41890	32785	27986	22531	17444	83,28	307	308,65
M2-0d-E	59649	45270	39193	30893	22139	74,23	333	335,05
M2-21d-A	60671	44875	40804	35132	22237	73,30	239	244,00
M2-21d-B	50551	38364	34935	31517	20293	80,29	253	255,55
M2-21d-C	47805	36742	35000	31877	19971	83,55	199	199,33
M2-21d-D	51622	38534	36189	33301	20310	78,69	220	221,43
M2-21d-E	44383	35240	33043	30316	19730	88,91	231	231,67
M2-42d-A	65970	48460	45317	39747	23701	71,85	231	231,43
M2-42d-B	37235	29314	26706	24113	16341	87,77	226	226,75
M2-42d-C	45738	34766	32693	29266	20050	87,67	242	244,50
M2-42d-D	44470	34477	32354	29508	20689	93,05	262	263,50
M2-42d-E	36716	27845	26175	24051	17942	97,73	242	243,67

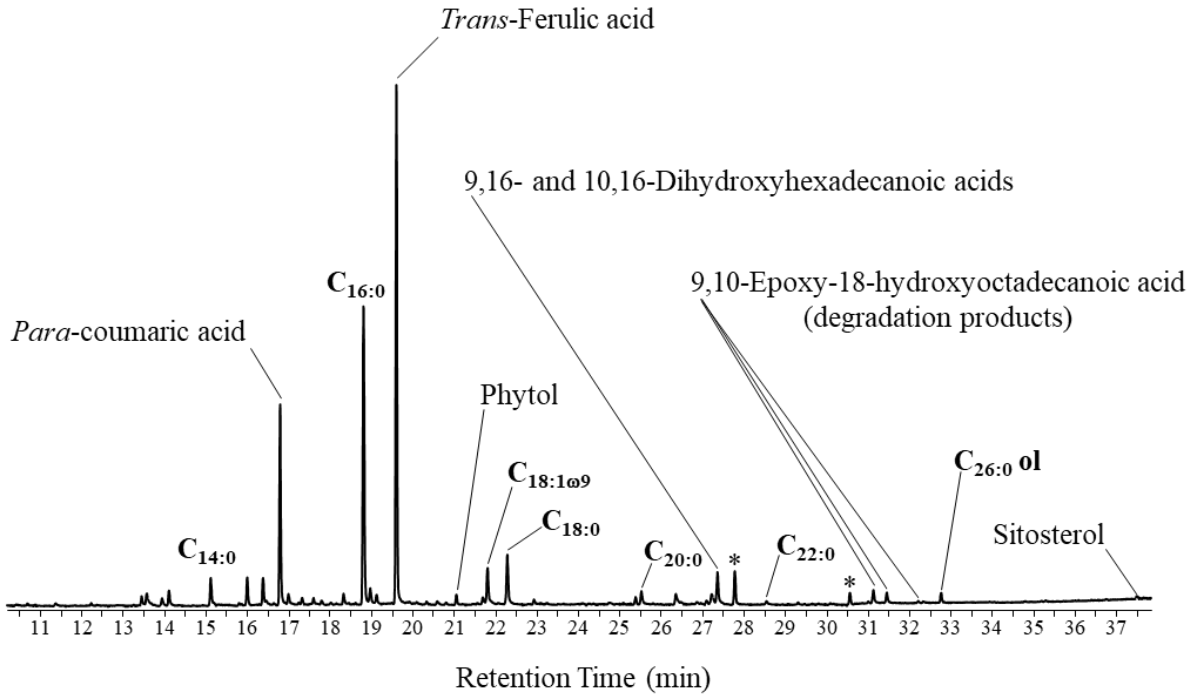

Fig. S1. Total ion current chromatogram of the total lipid extract of *A. sativa*.

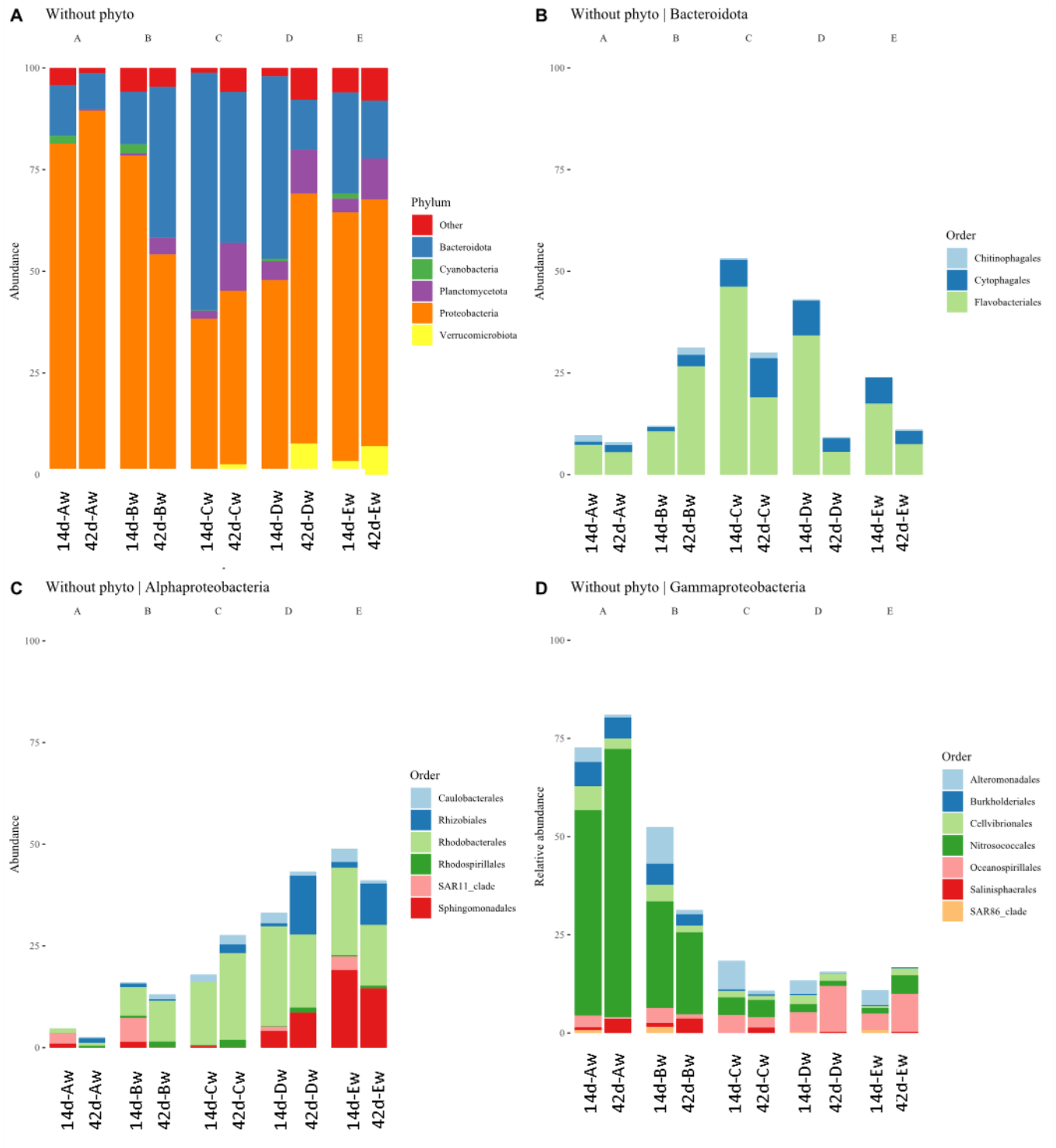

Fig. S2. Taxonomic affiliation of the 5 most abundant phyla (A), amongst the class of Gammaproteobacteria (B), amongst the class of Alphaproteobacteria (C) and amongst Bacteroidota (D) obtained from the 16*S* rRNA gene (DNA) sequences at different sampling times during the incubation without *S. costatum* as cosubstrate. The group "Other" contains all phyla with relative abundance lower than 1% of the total community.

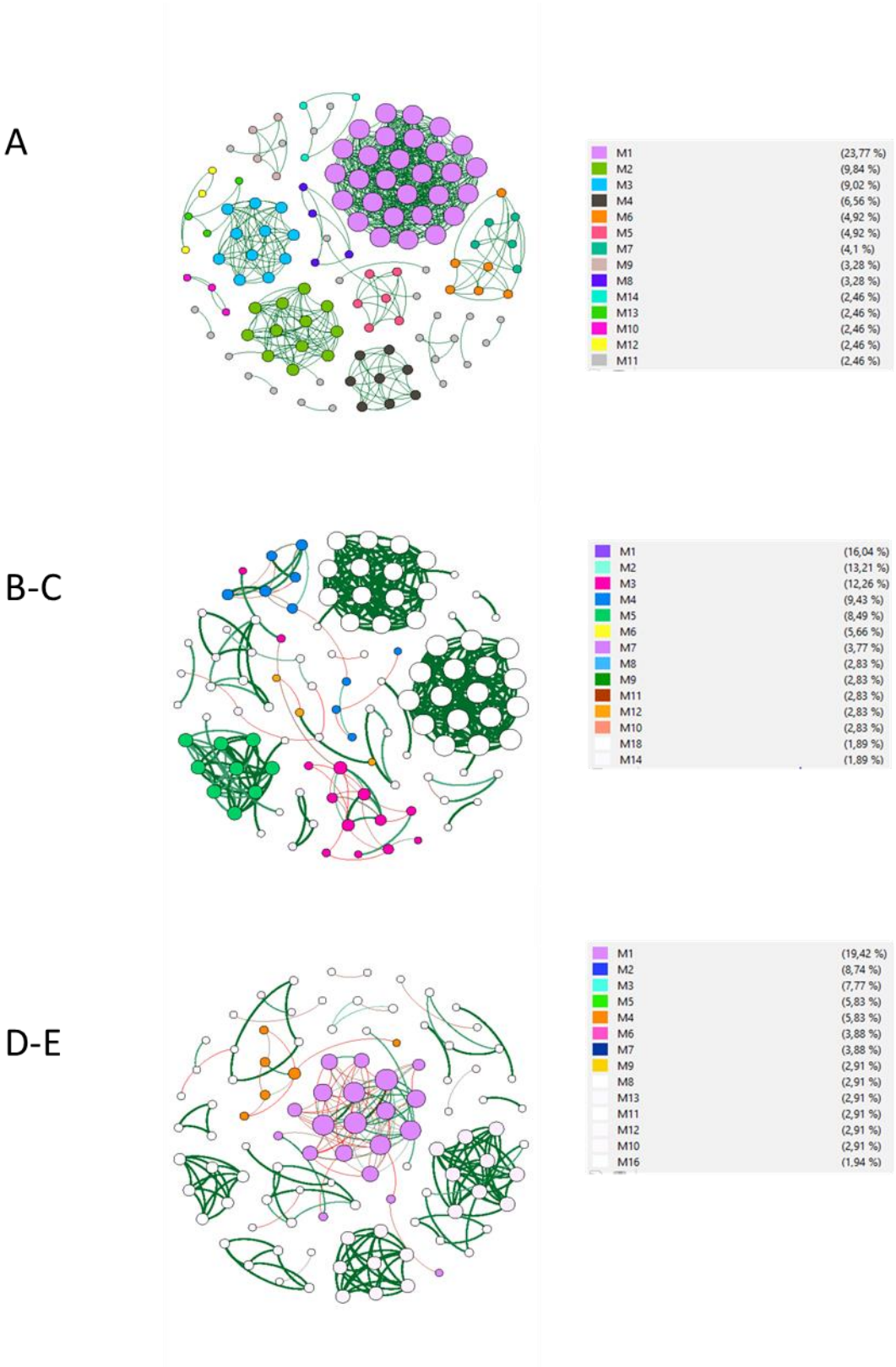

Fig. S3. Same network as in Figure 6. Modules significantly related to environmental parameters are colored.